

FINAL SCIENTIFIC/TECHNICAL REPORT DOE AWARD NO. DE-SC0018615, SBIR PHASE I

Project Title: Novel Design for High Field, Large Aperture Quadrupoles for Electron-Ion Collider

Report Date: 01/22/2019

Report Number: DOE-PBL-20190122

Company Name: Particle Beam Lasers, Inc.

Principal Investigator: Shailendra Chouhan

Purpose of Research, Research Carried Out, and Research Findings:

The Nuclear Science Advisory Committee (NSAC) constituted by the Department of Energy (DOE) Office of Nuclear Physics (NP) recommended that the proposed Electron Ion Collider (EIC) be the highest priority for new construction in the 2015 Long Range Plan (LRP) for Nuclear Science. The EIC requires development of several key technologies. The Phase I SBIR effort considered alternate techniques for efficient compensation of the external field generated by high field quadrupole and dipole magnets in the Interaction Region (IR). To achieve high luminosity, IR designs need a high field quadrupole (≥ 8 T pole tip field) for the heavier proton beams and an almost field free path (desired magnetic field within a few mT) for the electron beams which must travel very close to the quadrupole and dipole of proton beams.

The novel “modular design” concept explored in this study is based on simple racetrack coils. Magnets based on racetrack coils require less tooling and are generally less expensive to build. The modular quadrupole, like the Panofsky quadrupole, allows conductor at the mid-plane to be placed at a radius similar to the cosine two-theta magnets making it more efficient. This is crucial to creating the high field gradient necessary for the EIC IP quadrupoles.

We developed the modular design technology for the production of high field gradient quadrupoles for the IR of an EIC. We explored two modular design options that would be appropriate for the BNL Q1PF and the JLab QFFB1_US quadrupoles. Our analysis included both magnetic and structural designs for these quadrupoles.

Potential Applications of the Research:

The primary application of the research is to enable studies of fundamental physics in an electron-ion collider (EIC). By effectively shielding the electron beam path from the high fields present in the ion beam path, the electron beam can be tightly focused to maximize the number of interesting collisions in the EIC.

FINAL SCIENTIFIC/TECHNICAL REPORT DOE AWARD NO. DE-SC0018615, SBIR PHASE I

Recipient: Particle Beam Lasers, Inc.
18925 Dearborn Street
Northridge, CA 91324-2807

Sponsoring Program Office: Office of Science
U.S. Department of Energy

Project Title: Novel Design for High Field, Large Aperture
Quadrupoles for Electron-Ion Colliders

Principal Investigator: Shailendra Chouhan, PBL

Team Members: Ramesh Gupta, BNL
Michael Anerella, BNL
John Cozzolino, BNL
Stephen Kahn, PBL
James Kolonko, PBL
Delbert Larson, PBL
Ronald M. Scanlan, PBL
Robert Weggel, PBL
Erich Willen, PBL

SBIR/STTR Rights Notice (JAN 2015)

These SBIR/STTR data are furnished with SBIR/STTR rights under Award No. DE-SC0018615. Unless the Government obtains permission from the Recipient otherwise, the Government will protect SBIR/STTR data from non-governmental use and from disclosure outside the Government, except for purposes of review, for a period starting at the receipt of the SBIR/STTR data and ending after 4 years, unless extended in accordance with 48 CFR 27.409(h), from the delivery of the last technical deliverable under this award. In order for SBIR/STTR data to be extended by an SBIR/STTR Phase III award, the Recipient must properly notify DOE's Office of Scientific and Technical Information (OSTI) before the end of the previous protection period. After the protection period, the Government has a paid-up license to use, and to authorize others to use on its behalf, these data for Government purposes, but is relieved of all disclosure prohibitions and assumes no liability for unauthorized use of these data by third parties. This notice shall be affixed to any reproductions of these data, in whole or in part.

(End of notice)

Acknowledgment: This material is based upon work supported by the U.S. Department of Energy, Office of Science under Award Number DE-SC0018615.

Disclaimer: This report was prepared as an account of work sponsored by an agency of the United States Government. Neither the United States Government nor any agency thereof, nor any of their employees, makes any warranty, express or implied, or assumes any legal liability or responsibility for the accuracy, completeness, or usefulness of any information, apparatus, product, or process disclosed, or represents that its use would not infringe privately owned rights. Reference herein to any specific commercial product, process, or service by trade name, trademark, manufacturer, or otherwise does not necessarily constitute or imply its endorsement, recommendation, or favoring by the United States Government or any agency thereof. The views and opinions of authors expressed herein do not necessarily state or reflect those of the United States Government or any agency thereof.

Novel Design for High Field, Large Aperture Quadrupoles for Electron-Ion Collider

TABLE OF CONTENTS

Final Scientific/Technical Report DOE Award No. DE-SC0018615, SBIR Phase I.....	1
Final Scientific/Technical Report DOE Award No. DE-SC0018615, SBIR Phase I.....	2
Introduction	6
Modular Design Concept	6
Magnet Design Analysis	7
TABLE I: Requirements of the Interaction Region (IR) Magnets for the BNL and JLAB EIC	9
.....	9
Section A: Symmetric Magnet 2D Roxie Calculations.....	9
Table II Parameters that describe the designs considered.....	10
Table III Quench Margins for the symmetric designs A, B, and C.....	11
Table IV Harmonics Calculated with Roxie for the three symmetric configurations.....	12
Section B: Symmetric Magnet 2D and 3D Opera Calculations.....	13
TABLE V: Nb ₃ Sn Conductor Parameters Previously Used for LARP [7]	13
TABLE VI: Design and Extracted Parameters of the Quadrupole Calculated with Tosca.....	20
TABLE VII: Calculated Field Harmonics in the European Convention	20
TABLE VIII: Calculated Integrated Field Harmonics in the European Convention	21
Forces for Symmetric Design	23
TABLE IX: Force Vectors Acting on the Sections of each Coil-Packs. Units are in kN.....	23
TABLE X: Calculated Field Harmonics in the European Convention	26
Section C: Asymmetric Magnet 2D and 3D Design with Opera	27
TABLE XI: Comparison of Harmonics for Q1PF Calculated for 2D with 3D Harmonics Calculated at Axial Center of the Magnet.....	31
TABLE XII: Calculated Integrated Field Harmonics in the European Convention	32
Forces for the Simple Design	33
Table XIII: Forces on Simpler Design Coils in Newtons	33
Section D: Simpler Model Calculated with Roxie.....	34

Table XIV: Optimized Rotated Harmonics for the Simpler Quadrupole	35
Section E: Mechanical Design Analysis	35
Simpler Design	35
Assembly of the Simpler Design Magnet	39
Symmetric Design	41
Table XV	42
Section F: Concluding Remarks	44
References	45
Appendix: A.....	46
Coil with Split Turns Design.....	46

INTRODUCTION

This report outlines findings of the design work performed under the Small Business Innovation Research (SBIR) Phase I grant (DE-SC0018615) to Particle Beam Lasers, Inc. (PBL) and Brookhaven National Laboratory (BNL) to develop a novel modular design for Electron-Ion Collider (EIC) quadrupoles based on racetrack coils, which needs less expensive tooling to build, particularly as compared to the commonly used Cosine Two Theta magnets in high energy accelerators. There are two versions of the modular designs that we have investigated which we have named – Simpler and Symmetric. The findings of each design are presented in the later section of the report. The simpler design is based on four sets of racetrack coils where the current is returned on one side of the magnet as shown on the left side of Fig. 1. It lacks the eight-fold quadrupole symmetry in the cross-section and therefore in addition to the normal field harmonic components that are allowed by quadrupole symmetry, one would also expect certain *non-allowed* skew harmonic components. The symmetric design shown on the right side of Fig. 1 is based on eight sets of racetrack coils that splits the return current between the left hand and right-hand sides. This design has quadrupole symmetry in the cross-section. For the symmetric design to maintain quadrupole symmetry and achieve the needed field integration some of the modules of one of the coils must interleave another one at the magnet ends; details are shown in a later section. Nevertheless, both designs use similar length of conductor and almost double the length compare to the conventional cosine-two-theta quadrupole design. An advantage of the modular design is that it also enables the same coils to be used in model magnets over a range of apertures. Such a modular design may greatly facilitate R&D and reduce its costs, which often dominate the total cost of magnets that are limited in numbers. We carried out the detailed magnetic design calculations for the quadrupoles of the interaction region (IR) for a future Electron-Ion Collider (EIC) as proposed by two national labs, Brookhaven National Laboratory (BNL) and Thomas Jefferson National Accelerator Facility (TJNAF) or simply Jefferson Lab (JLab).

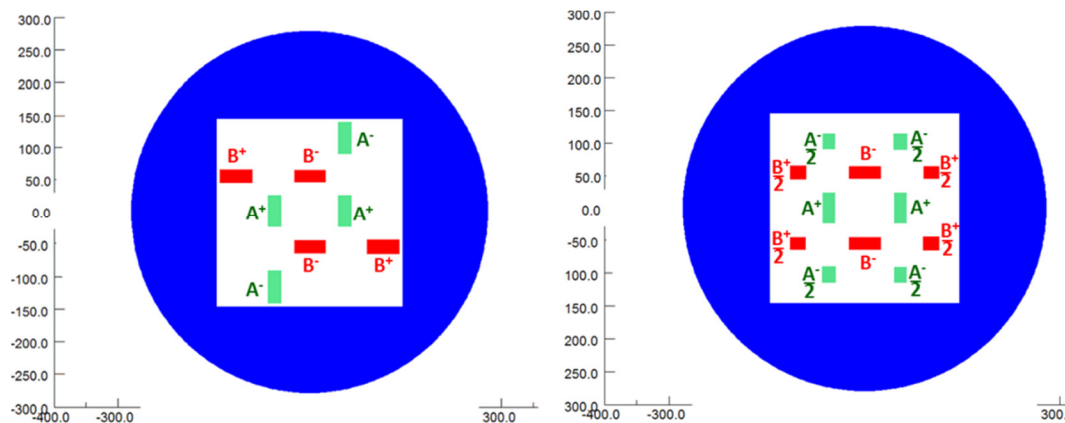


Fig. 1: Sketch of modular designs proposed. On the left is the simpler design and on the right is the symmetric design.

MODULAR DESIGN CONCEPT

The modular design shown in Fig. 1 is based on simple racetrack coils placed in a quadrupole configuration. The coil configuration close to the bore is similar to the Panofsky quadrupole [1]. This configuration has the advantage that the conductor placed at the mid-plane in each quadrant is at the minimum coil radius, which is most efficient as it contributes the most field. We refer to these designs as

“modular designs” because these racetrack modules can be arranged for different model quadrupoles of the machine for a fast-turn-around and low-cost quadrupole magnet R&D program. The modular design offers a unique opportunity to change the quadrupole apertures while using the same coil modules. The simplified 2d drawing of the symmetric design shown in Fig. 2 demonstrates the first-quadrant coil translations to increase the aperture of the magnet (left) by moving coil A+ to the right and coil B+ to upwards by the same amount.

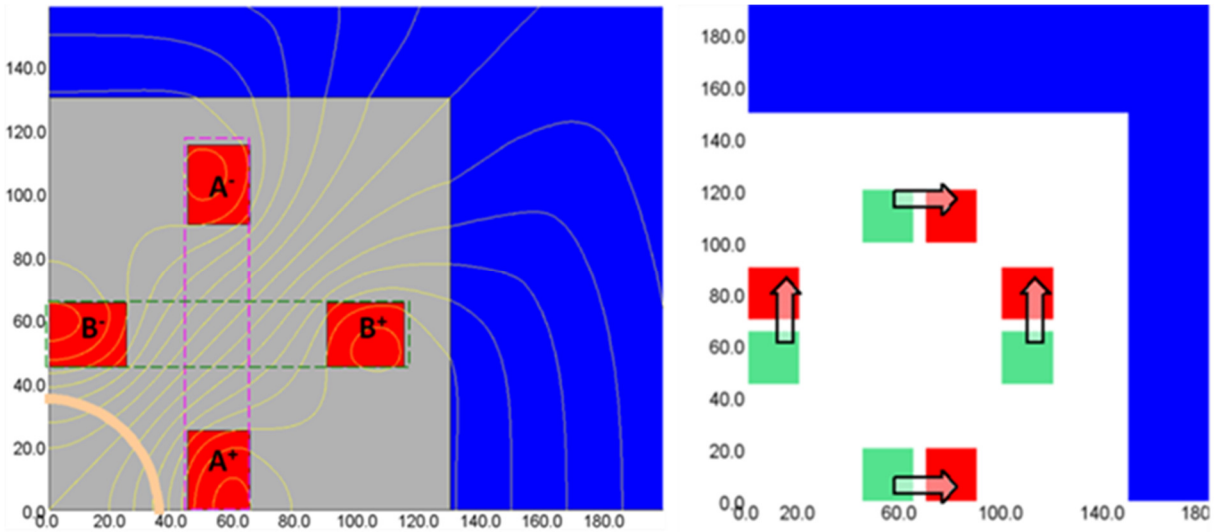


Fig. 2: Modular designs offer a valuable R&D opportunity to increase the magnet aperture from the figure at the left to that at the right by moving racetrack coil A to the right and coil B upwards by the same amount.

MAGNET DESIGN ANALYSIS

We performed the magnetic design calculations for the following EIC quadrupoles which requires the high field gradient and the use of Nb3Sn coils: (a) BNL Q1PF, (b) JLab QFFB1_US, (c) JLab QFFB2_US, (d) JLab QFFB3_US. The proposed layouts of the interaction region (IR) for the eRHIC and JLeic designs is shown in Fig. 3. The design specifications of the magnets, as available at the time of proposal, are shown in Table I [2-4]; a design was performed for the highlighted magnets. The design approaches carried out for the Q1PF magnet were: the simpler and the symmetric modular design. These approaches will be discussed [5]. In the case of symmetric design, the same racetrack coil cross-section can be used as well for JLab’s quadrupoles with differences in field gradient, aperture and other design parameters. It is projected that the modular design will reduce the project costs of the EIC by minimizing the R&D and tooling costs required for each magnet, particularly when only one of each kind is needed.

Another design requirement which is unambiguous, that these high field gradient quadrupoles (with adequate margin of at least 20 %) must also simultaneously ensure along with the field quality that there is a nearly field free region for the passage of the electron beam in the interaction region [IR] of the EIC.

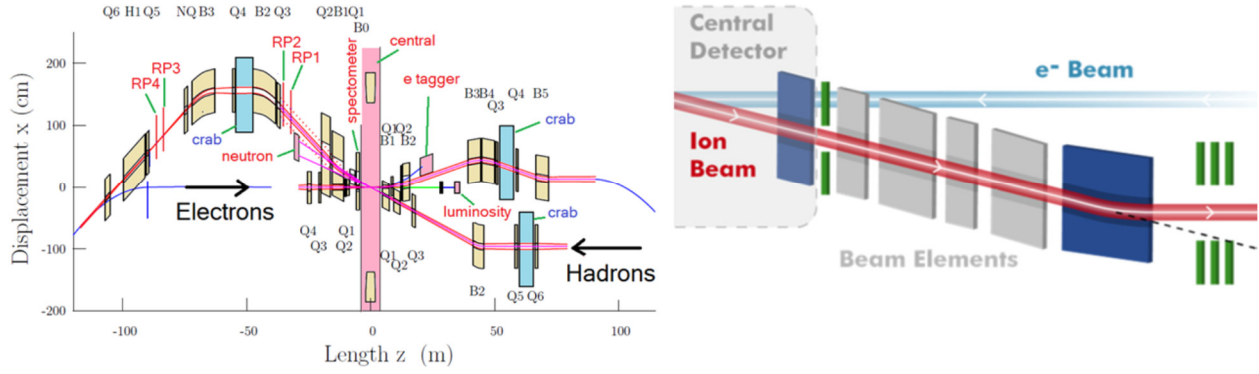


Fig. 3: Proposed layout of the Interaction Region of eRHIC (BNL) on the left and the JLeic (JLab) on the right.

TABLE I: Requirements of the Interaction Region (IR) Magnets for the BNL and JLAB EIC

BNL Requirements							
Hadron Forward Side							
Name	Beam	Position entrance[m]	Length [m]	Strength	Full Aperture entrance [mm]	Full Aperture exit [mm]	Coil Type
B0PF	hadrons	5.	1.2	1.3 T	500×240	500×240	s.c.NbTi
Q1EF	electrons	5.0	1.2	14.6 T/m	22	22	s.c. NbTi
Q1PF	hadron	6.8	1.5	131 T/m	84	84	s.c. Nb ₃ Sn
Q1PF Shield	electrons	6.8	1.5	N/A	N/A	N/A	s.c. NbTi
Q2EF	electrons	8.74	1.72	6.0 T/m	48.5	48.5	s.c. NbTi
Q2PF	hadrons	11.1	2.4	45 T/m	210	210	s.c. NbTi
B1PF	hadrons	13.9	3.0	4.47 T	204	244	s.c. NbTi
Hadron Rear Side							
Name	Beam	Position [m]	Length [m]	Strength	Full Aperture entrance [mm]	Full Aperture exit [mm]	Coil Type
Q1ER	electrons	5.5	3.42	5.1 T/m	135	186	s.c. NbTi
Q1PR	hadrons	5.5	3.42	82.9 T/m	42	68	s.c.NbTi
Q2ER	electrons	11.67	2.57	4.23 T/m	228	266	s.c.NbTi
Q2PR	hadrons	11.67	2.57	54.86 T/m	90	110	s.c.NbTi
B2ER	electrons	19.2	4.0	0.09 T	281	338	s.c.NbTi

JLAB Requirements								
Magnet Location	Magnet Type	Magnet Strength	Magnetic length	Distance from the	Good field	New Inner Radius	Outer radius (cm)	Angle between ion & electron beam line (mrad)
Interaction Region Ion (IR)	Quadrupole QFFB3_US	-116	1	-7.70	3 cm	4	12	50
	Quadrupole QFFB2_US	149	1.5	-6.00	3 cm	4	12	50
	Quadrupole QFFB1_US	-141	1.2	-4.20	2 cm	3	10	50
	Quadrupole QFFB1	-88	1.2	7.60	4 cm	8.5	17.1	50
	Quadrupole QFFB2	51	2.4	10.40	4 cm	12.6	24.7	50
	Quadrupole QFFB3	-35	1.2	13.20	4 cm	14.8	26.7	50
Interaction Region Electron (IR)	Common Quad design based on new requirement January 2018, combined with Skew Quads	Quad 45 (varies from 13.63 to 44.78)	0.6	-4.9 -3.7 -2.5 3.26 4.46 6.91	3.2	4.5	8	50

SECTION A: SYMMETRIC MAGNET 2D ROXIE CALCULATIONS

We have optimized three configurations of the symmetric design using the Roxie program [6]. The three designs are pictured in Fig. 4 with configuration parameters given in Table II. Design A divides the coils into two layers with 28 turns each (not including the return) and each turn carries 9.3 kA. Design B also has two layers but adds an extra turn at the pole. Design B has 35 turns carrying 12.7 kA. Design C has a single layer with 27 turns carrying 17 kA in each turn. Design D will be addressed later as the simpler design. Each configuration was optimized by varying the position of, and gaps between, the coil blocks to reduce harmonics higher than the fundamental b_2 . Also, in choosing the most appropriate configuration the quench margin is considered. Fig. 5 shows the $|B|$ field in the inner coils of the three

symmetric configurations. The peak field occurs on the inner surface at the end of the coils. Table III compares the peak field at the coils with the quench field for the different symmetric configurations. The Roxie program calculates the quench current based on the characteristics of the superconductor. Table III shows the values of the coil block with the largest ratio of peak field to quench field (load line ratio).

Table IV shows the harmonics calculated by Roxie for the three symmetric configurations. The harmonics are given relative to the dominant quadrupole harmonic (n=2) represented by B_{R0} in the following formula used to define the field in terms of the harmonics:

$$B_y + iB_x = 10^{-4} \times B_{R0} \sum_{n=1}^{\infty} (b_n + ia_n) [(x + iy)/R_{ref}]^{n-1}$$

where B_x and B_y are the components of the field at (x, y) and R_{ref} is the reference radius where the harmonics are calculated. Typically, a good field design has harmonics less than one unit which is consistent with magnet fabrication errors. Configuration C has the best field quality but also carries the largest conductor current and consequently operates closest to quench conditions as shown in Table III. Configuration C does not meet the 20% adequate current margin set as a goal in the phase I proposal. This can be rectified by choosing a different conductor with a larger cross section area.

Table II Parameters that describe the designs considered

. Designs A, B, and C are symmetric designs and design D is the simpler design.

Case	Layers	Blocks	Turn Configuration	Turns w/ return	Current in turn Amps
A	2	7	28+28	112	9300
B	2+	8	1+18+16	70	12700
C	1	7	27	54	17000
D	1	5	2×(3+8+7+4+3)	50	17200

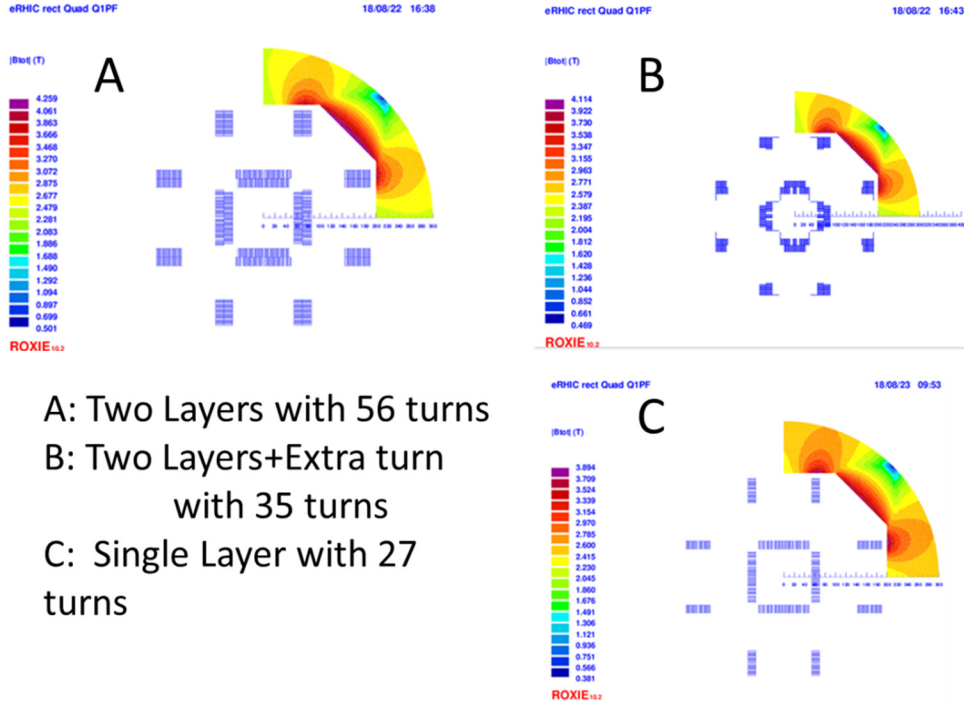


Fig. 4: Three versions of the symmetric design that have been optimized.

Table III Quench Margins for the symmetric designs A, B, and C.

Design	Current I, Amps	Peak B , T	Quench B , T	% Load Line	% Short Sample
A, symm	9008	9.7	15.5	62.7	58.6
B, symm	12700	9.1	12.5	72.8	29.4
C, symm	17000	10.4	11.7	88.2	19.4
D, simp	17073	10.4	11.8	88.7	18.7

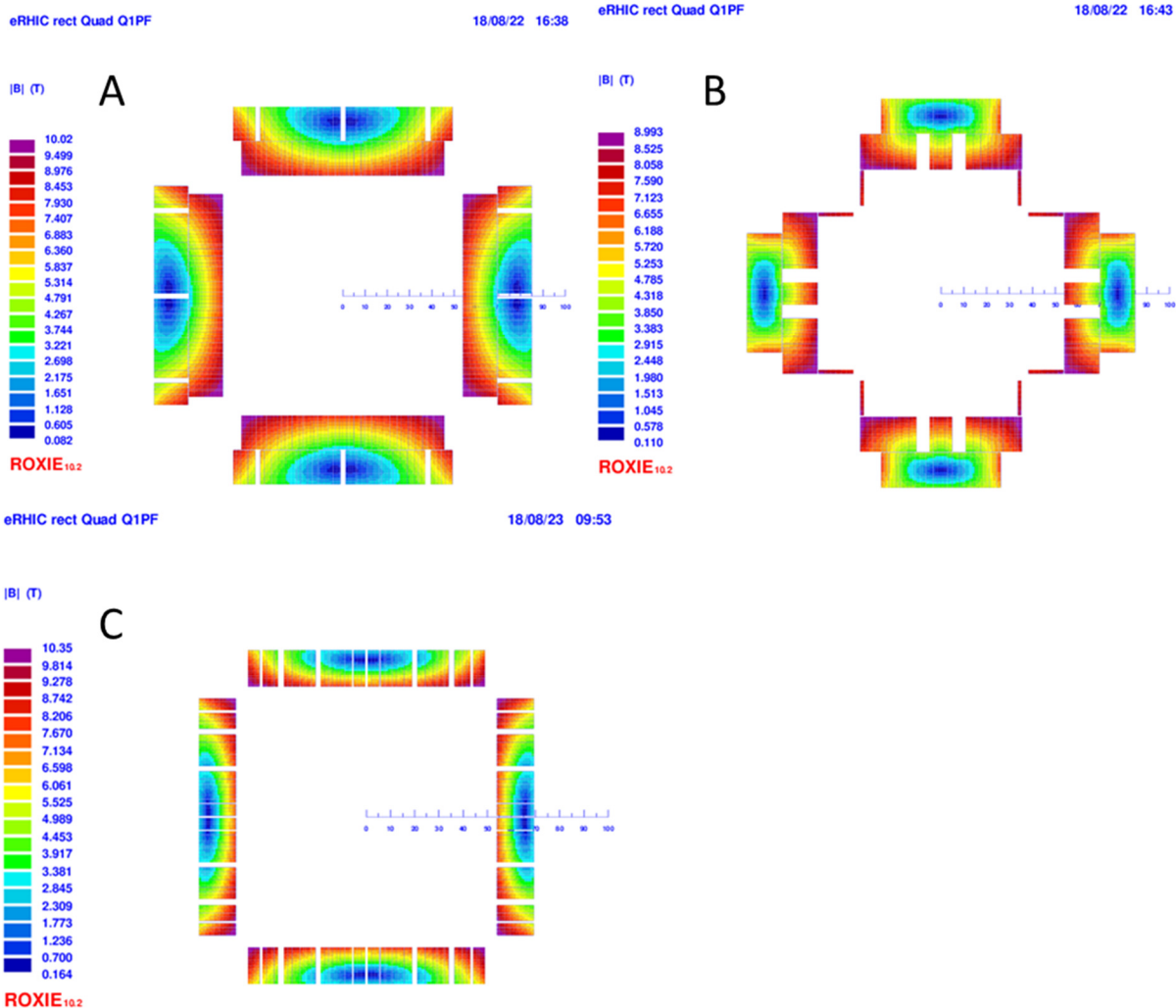


Fig. 5: Field in inner coils at the design current for designs A, B, and C

Table IV Harmonics Calculated with Roxie for the three symmetric configurations.

Order	A	B	C
2	10000	10000	10000
6	-1.15457	-1.40205	0.02106
10	-1.60786	1.21855	-0.00048
14	0.04272	-0.02917	-0.36019
18	-0.00393	0.6533	-0.12193
Gradient	140.154 T/m	139.8871 T/m	140.0002 T/m
Field at R_{ref}	5.0456 T		5.04009 T

SECTION B: SYMMETRIC MAGNET 2D AND 3D OPERA CALCULATIONS

As a parallel activity, the OPERA 2D and 3D program was used to perform optimization of symmetric coil configuration and the optimized coil configuration is different from the design discussed in the section-A. A 2D parametric finite element model was first created to minimize the time intensive 3D calculations. The mass of the yoke and cross-section of the superconducting coil were optimized while keeping field quality over the operating range. The optimized cross-section of design B of the BNL Q1PF is shown in Fig. 6. We proposed the use of a similar coil cross-section for the several other JLAB upstream magnets of the IR section. In the optimized coil configuration, the parameters of the proposed Nb₃Sn cable are identical to the previously used cable in the fabrication of the LARP quadrupole magnet. The parameters of the Nb₃Sn cable are summarized in Table V [7].

Figure 6 shows an OPERA2d model of an octant of the *symmetric* two-layer coil design with an additional two-turn pole coil, iron yoke and the surrounding air region indicated for the quadrupole Q1PF magnet. The position of the conductor in the coil is optimized to achieve and meet the field quality requirements. It also shows part of the iron yoke containing a rectangle cutout for the electron beam pipe. The yoke cross-section is optimized to minimize the fringe field magnitude in the electron beam region. The center of the electron beam pipe is 180 mm from the magnet center.

Figure 7 shows an OPERA2d field contour plot for the Q1PF quadrupole design. The design field gradient for Q1PF is 140 T/m (with at least 20 % margin), and the coil aperture is 96 mm. The peak field magnitude in the coil is around 10.2 Tesla whereas the peak magnitude of the field in the iron is around 5.4 Tesla. It also shows a reduced field region in the cutout section of the return yoke for the electron beam. The yoke cross-section is optimized to minimize the field magnitude in the electron beam region. The Q1PF quadrupole model provides a field gradient of 150 T/m and a peak field at the pole ($r = 0.036$ m) of 5.4 T. The model also provides information about the Lorentz forces on the coil, stored energy and the magnitude of higher harmonics in the center of the magnet. The quadrupole field components (B_Y and B_{MOD}) profile along the radial axis are shown in Fig. 8. The linear field region in the center of the magnet provides the required high field gradient for the proton/ion beam. The field at 180 mm inside the cutout in the yoke for the electron beam is 0.306 T.

TABLE V: Nb₃Sn Conductor Parameters Previously Used for LARP [7]

Strand Diameter (mm)	0.8
Cu to non-cu ratio	1.17
Number of strands	35
Cable insulation (mm)	0.1
Cable width, bare (mm)	15.15
Mid-thickness (mm)	1.437
Keystone angle	0.
Cable width insulated (mm)	15.35
Mid-thickness insulated (mm)	1.637
Cable Jc (4.4K, 13.54 T), A/mm ²	2087

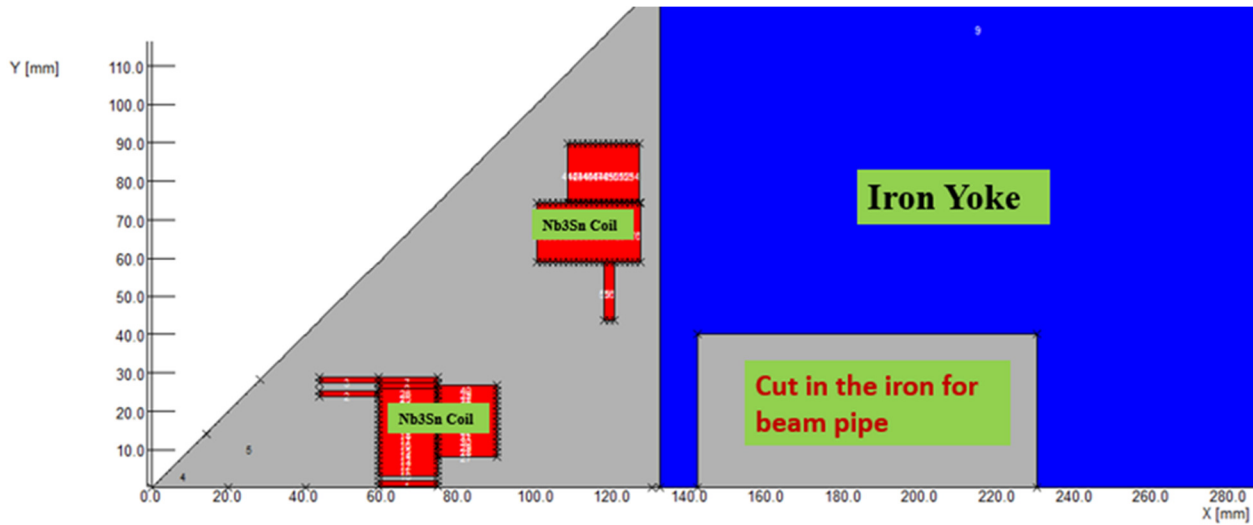


Figure.6: OPERA2d model of an octant of the symmetric modular design (configuration B) with two layers of optimized coils, in addition to a two-turn pole block. Return coil blocks are further away from the aperture. The rectangle cutout in the iron return yoke is for the electron beam pipe.

To analyze the 3D behavior of the magnet design, especially the flux distribution along the beam axis, the stray field in and along the electron beam pipe, the peak field in the coil area, the integrated higher harmonic contents, and the forces on the coil, a magnetic model for TOSCA was developed. Figure 9 shows the 1/16th 3D meshed model of the BNL_QIPF quadrupole with coils and the surround air region. Figure 10 shows a schematic layout for quadrupole magnet with coils and cutout in the return yoke (dimensions are in cm). Each quadrant of the magnet encompasses a set of two orthogonal coils. To avoid the two orthogonal coils overlapping in the end region, the length of one of the coils is made smaller than the other one. The outcome of this arrangement results in perfect quadrupole symmetry in the longitudinal center but the coils lack symmetry at the ends due to the different coil lengths. To overcome the lack of symmetry at the ends and achieve the desired field integral in both planes, segments of one of the coils have different lengths and enclose the other orthogonal coil at the ends, as shown in Fig. 11. (Schematic of the simplified version of the two-coil arrangement is shown for better understanding.) Fig. 11 shows the length of one of the coil pancakes of the double coil pancake made longer while the other coil pancake is made shorter so that the orthogonal coil can be inserted between the two pancakes. This is one option to overcome the inbuilt lack of symmetry at the coil ends.

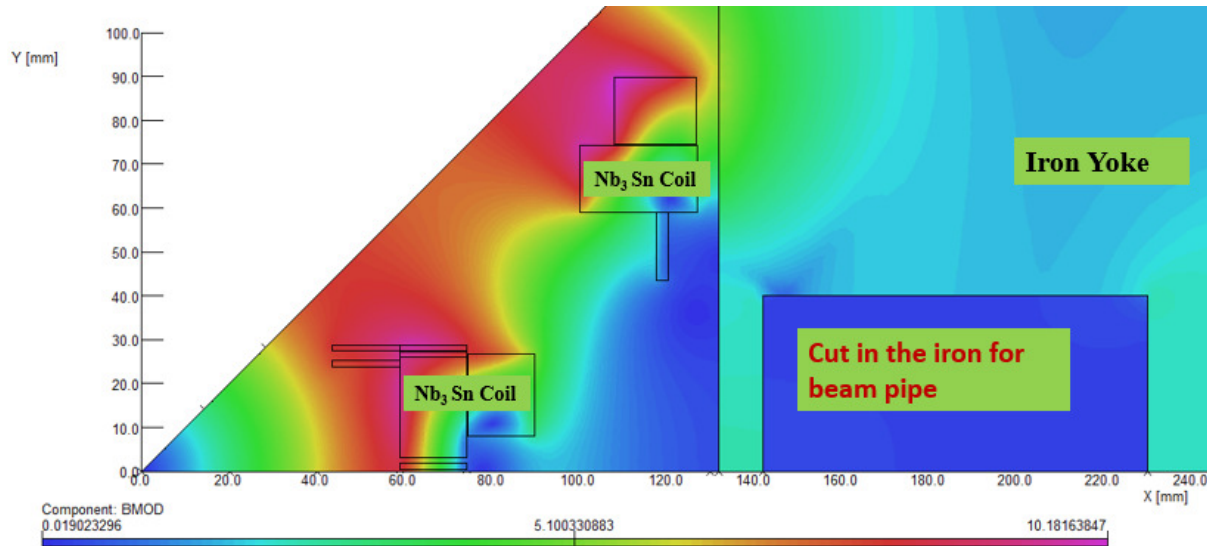


Figure 7: OPERA2d contour plot of $|B|$ for an octant of the symmetric modular design B with two layers of coils, in addition to a two-turn pole block. Return coil blocks are further away from the aperture. The rectangle cutout in the iron return yoke is for the electron beam pipe.

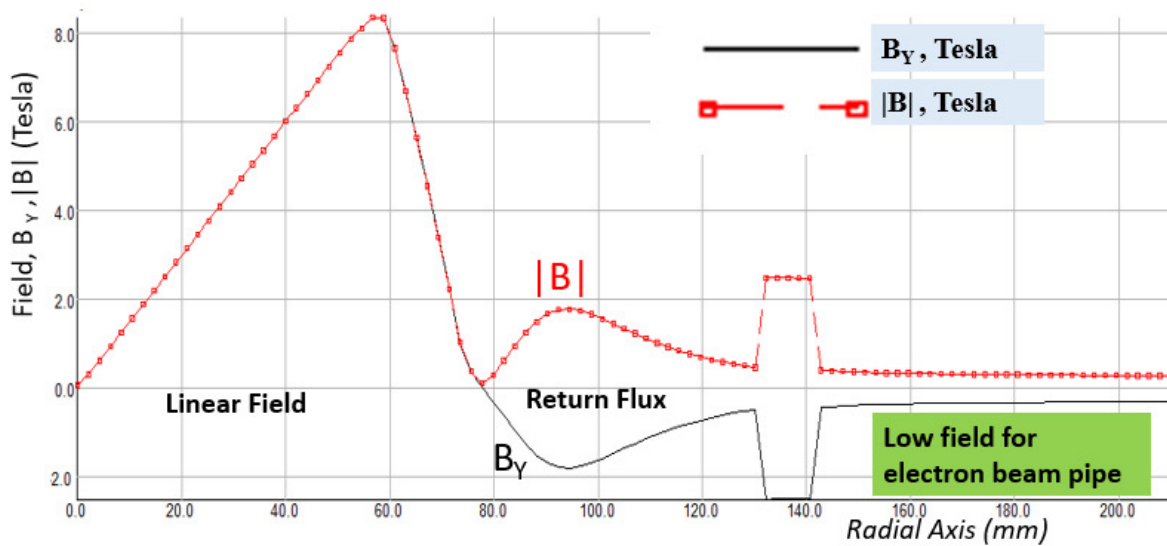


Figure 8: Profile of the calculated field components (B_y and B_{MOD}) along the mid-plane axis. The magnitude of the field at a radius of 0.036 m is 5.4 tesla whereas the magnitude of the field at 180 mm is around 0.306 tesla.

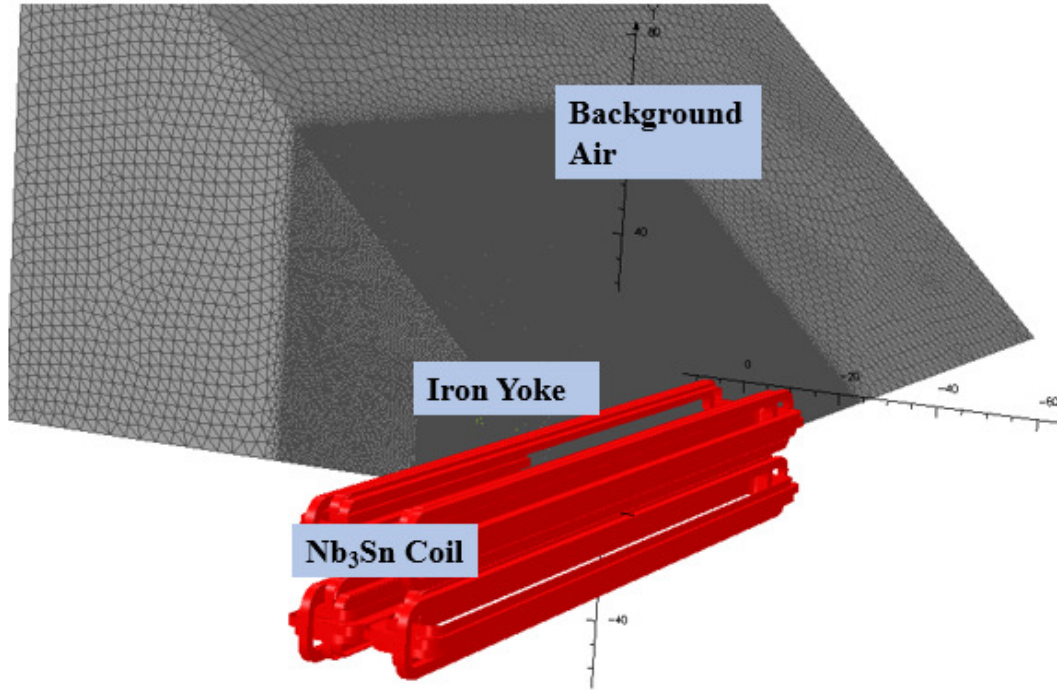


Figure 9: 3d meshed model for the superconducting Q1PF quadrupole magnet with coils, return yoke and background air (dimensions are in cm).

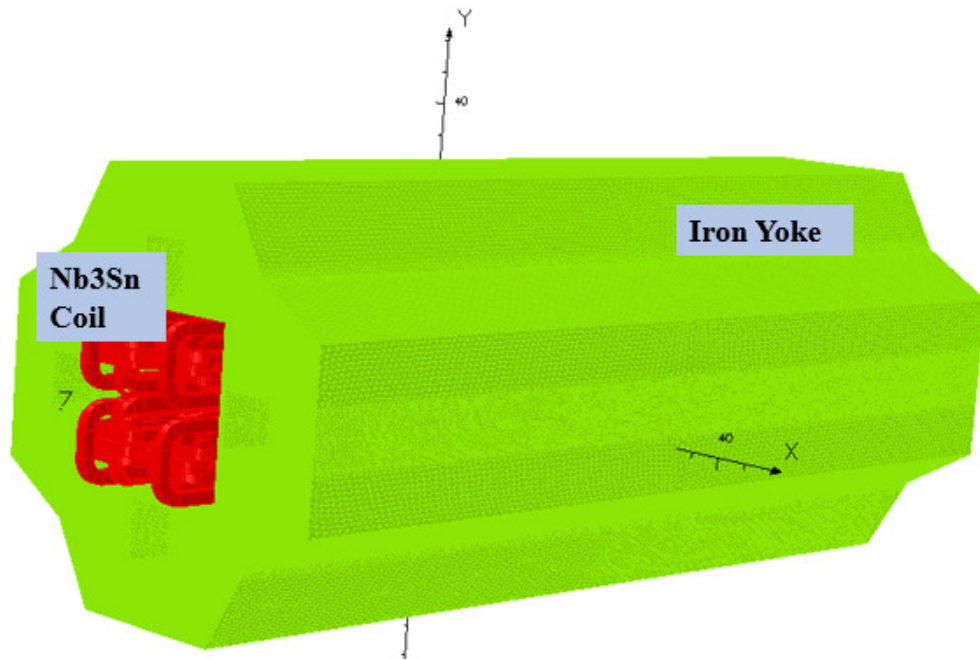


Figure 10: Schematic layout for the superconducting Q1PF quadrupole magnet with full set of coils.

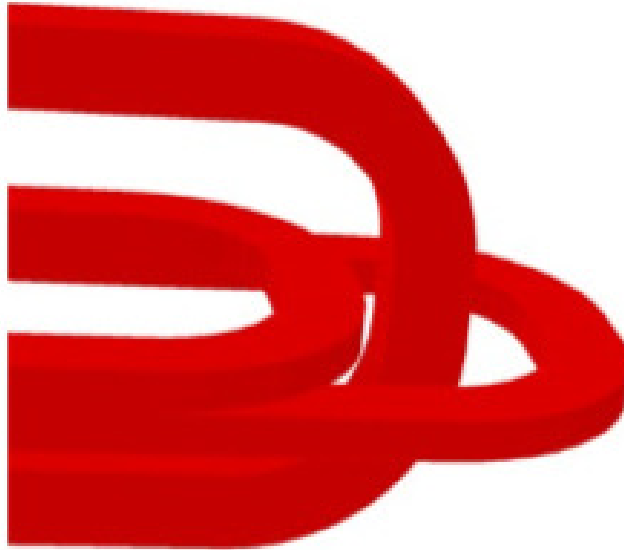


Figure 11: Schematic layout for the superconducting coils in the end region (simplified version for better understanding). The length of each of the coil pancakes of the double pancake coils is adjusted to accommodate the other orthogonal coil. This is one of the options to overcome from the inbuilt lack of symmetry at the ends. One can also achieve the desired field integral in both planes via fine-tuning of the coil length.

The calculated integrated field strengths, $\int B_{2X} \cdot dL$ and $\int B_{2Y} \cdot dL$ at the reference radius of 36 mm are 8.32 T-m and 8.35 T-m respectively. The discrepancy between the two-field components is around 0.4%. A field plot along the longitudinal axis at a radius of 36 mm is shown in Fig. 12. Adjustments to the coils may be necessary to equalize these integrated field strengths.

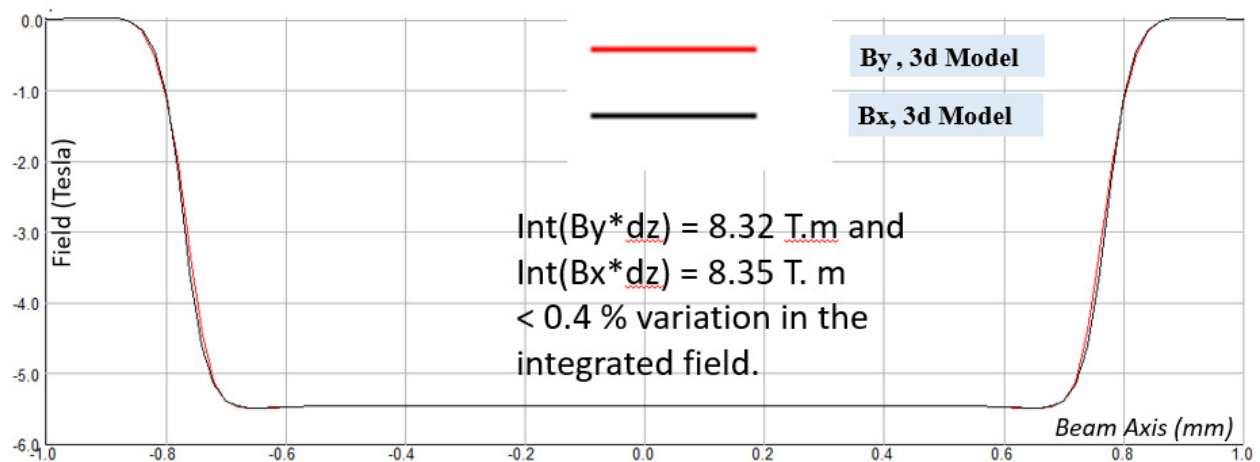


Figure 12: Calculated field profile along the longitudinal axis at the radius of 36 mm. The length of the two orthogonal coils is adjusted to achieve the desired field integral in both planes. The difference in the magnitude of integral field of the components is below 0.25%.

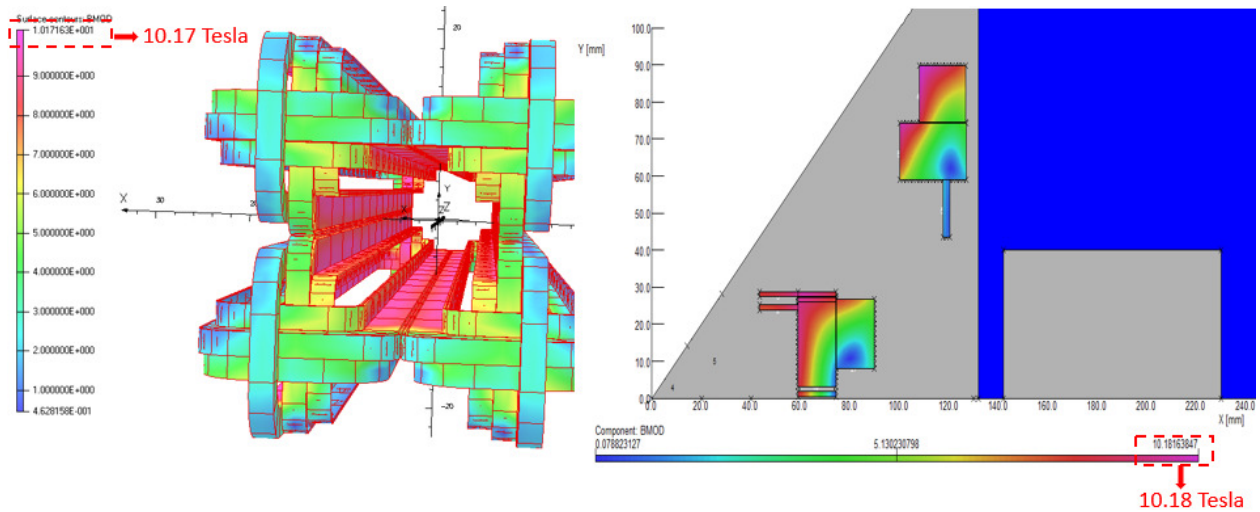


Figure 13: Field contour on the conductor surface of the Symmetric Q1PF modular design. The peak field magnitude in the conductor is 10.18 tesla.

Based on the 2d and 3d design a detailed analysis has been performed and the important results were compared. The field contour on the surface of the *symmetric* Q1PF quadrupole conductor is shown in Fig. 13. Both 2d and 3d results suggest a 10.18 Tesla peak field magnitude. Field data (B_Y and B_{MOD}) along the mid-plane axis of the 2d and 3d model is compared in Fig. 14, and the results of the two models agree. Other important design and extracted parameters from the 2d and 3d quadrupole model are included in Table VI.

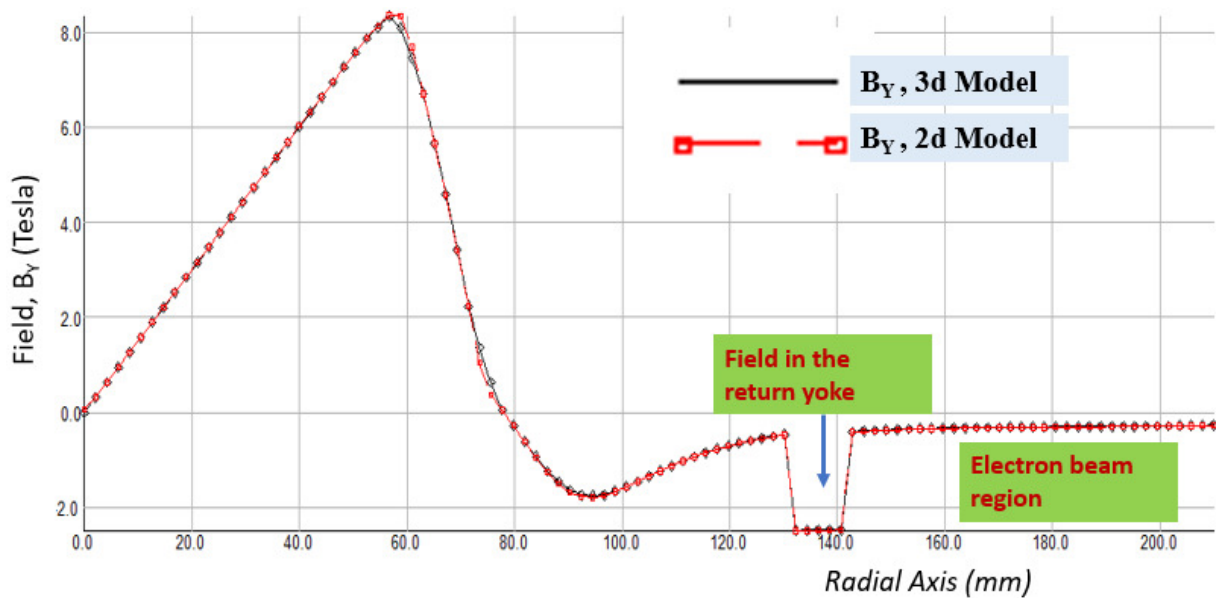


Figure 14a. Calculated field, B_Y (T) results from 2d and 3d model compared along the mid-plane axis. (Units are in millimeter and tesla).

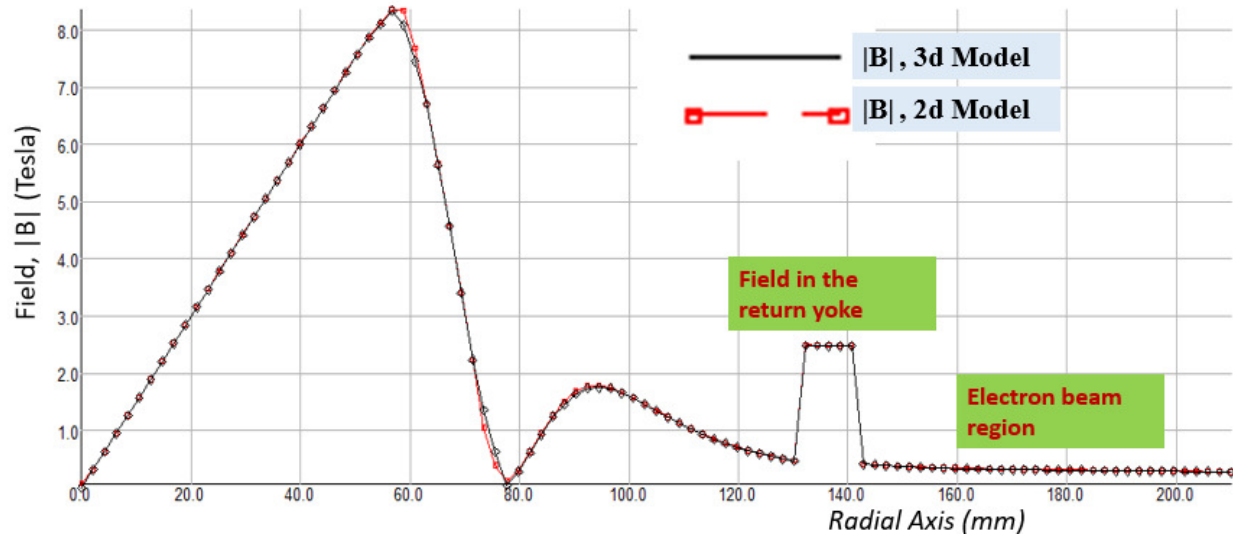


Figure 14b: Calculated field, $B_{MOD}(T)$ results from 2d and 3d model compared along the mid-plane axis. (Units are in millimeter and tesla)

Fig. 15 shows the relative amplitude of higher harmonics in the center of the *symmetric* Q1PF quadrupole from the 2d and 3d model analysis. The harmonics were analyzed at each excitation current of the magnet. To limit the large value of b_6 and b_{10} over the operating range of the large field gradient Q1PF quadrupole coil optimization has been performed. In the 2d model optimization achieved a value for the higher harmonics that is within the design specification and based on the information 3d modeling was performed. The values of the first few allowed higher harmonics in the center of the magnet at peak operating field are given in Table VII. As a different optimization procedure was performed for the OPERA2D analysis the harmonics are expected to be different from those in Table IV for the Roxie case B. The harmonics of the 3D model in Table VII were calculated at the axial center of the magnet. The aspects of the 3d design such as integrated harmonics were analyzed from the data construed from the model. The values of the first few allowed integrated higher harmonics and integral field strengths at maximum field are given in Table VIII. Along with the allowed harmonics of quadrupole field such as b_6 , b_{10} , $b_{14}...$, $b_{(2n+2)}$, the non-allowed octupole and its higher components are present. The large value of b_4 in the Symmetric Q1PF quadrupoles is due to the unbalanced shape of the coils at the ends. The relative amplitudes of the higher harmonics (integrated and in the center) with respect to the quadrupole component are shown in Fig. 16.

TABLE VI: Design and Extracted Parameters of the Quadrupole Calculated with Tosca

Quantity	Q1PF (BNL)
Number of Magnets	01
Max. field at 75 % of warm bore (T)	5.4
Max. field gradient (T/m)	150
Magnetic yoke Length (m)	1.5
Warm bore diameter (mm)	96
Number of turns per octant	72
Operating current (A)	12880
Eng. Current density (A/m ²)	6.25 x 10 ⁸
Effective length (m)	1.54
Stored energy at operating current (MJ)	1.503
Self-inductance at operating current (H)	0.018

TABLE VII: Calculated Field Harmonics in the European Convention

Harmonic #	Q1PF (2D design)	Q1PF (3D design)
$\int B_2 * dL$	--	--
b_6	-2.22E-05	5.50E-04
b_{10}	-9.45E-05	-5.61E-05
b_{14}	1.25E-05	1.58E-04
b_{18}	1.63E-04	-5.53E-05
b_{22}	-1.26E-04	2.36E-05

Harmonics for the 3D model were calculated at the longitudinal center of the magnet. Reference radius is 36 mm (75 % of the warm bore). $\int B_2 * dL$ is integrated field strength in T·m. The other components relative to the quadrupole field value in the center.

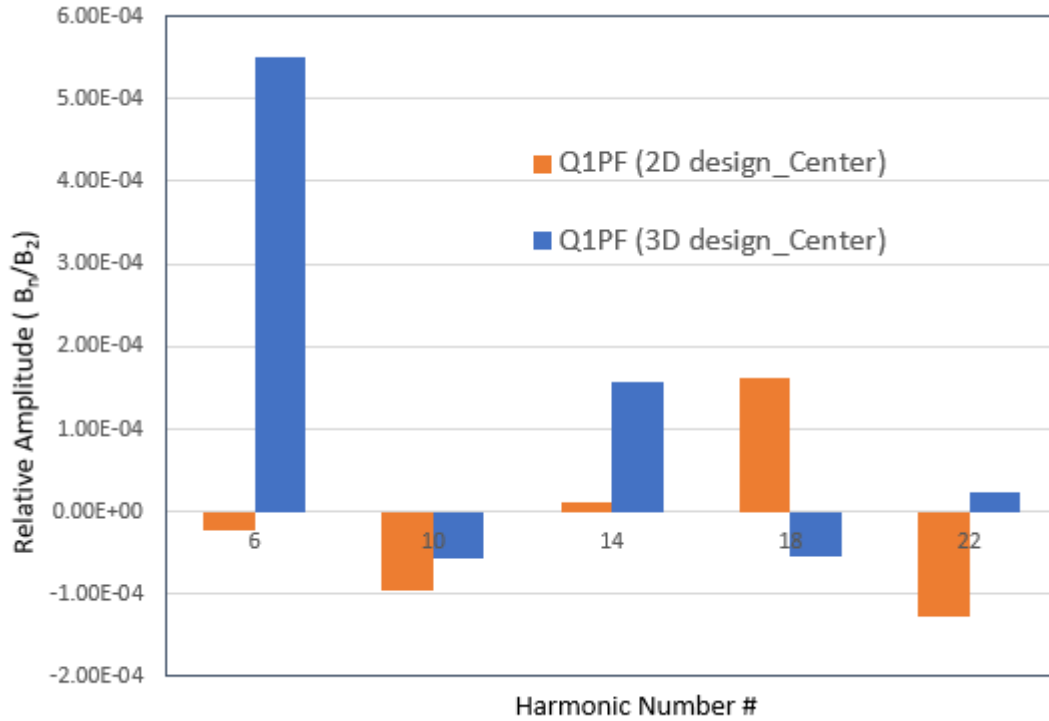


Fig.15. Relative amplitude of the higher harmonics with respect to the quadrupole component for 150 T/m field gradient of Q1PF quadrupole.

TABLE VIII: Calculated Integrated Field Harmonics in the European Convention

Harmonic order	Q1PF (3D design) <i>INTEGRATED</i>	Q1PF (3D design) <i>AXIAL CENTER</i>
$B_{2(x,y)}*dL$	8.32 / 8.35	--
b_4	$-1.76E-03$	$3.70E-06$
b_6	$3.00E-04$	$5.50E-04$
b_{10}	$-8.39E-05$	$-5.61E-05$
b_{14}	$1.55E-04$	$1.58E-04$
b_{18}	$-7.57E-05$	$-5.53E-05$
b_{22}	$2.88E-06$	$2.36E-05$

Reference radius is 36 mm (75 % of the warm bore). B_2*dL is integrated field strength in T·m. The other components relative to the quadrupole field value in the center.

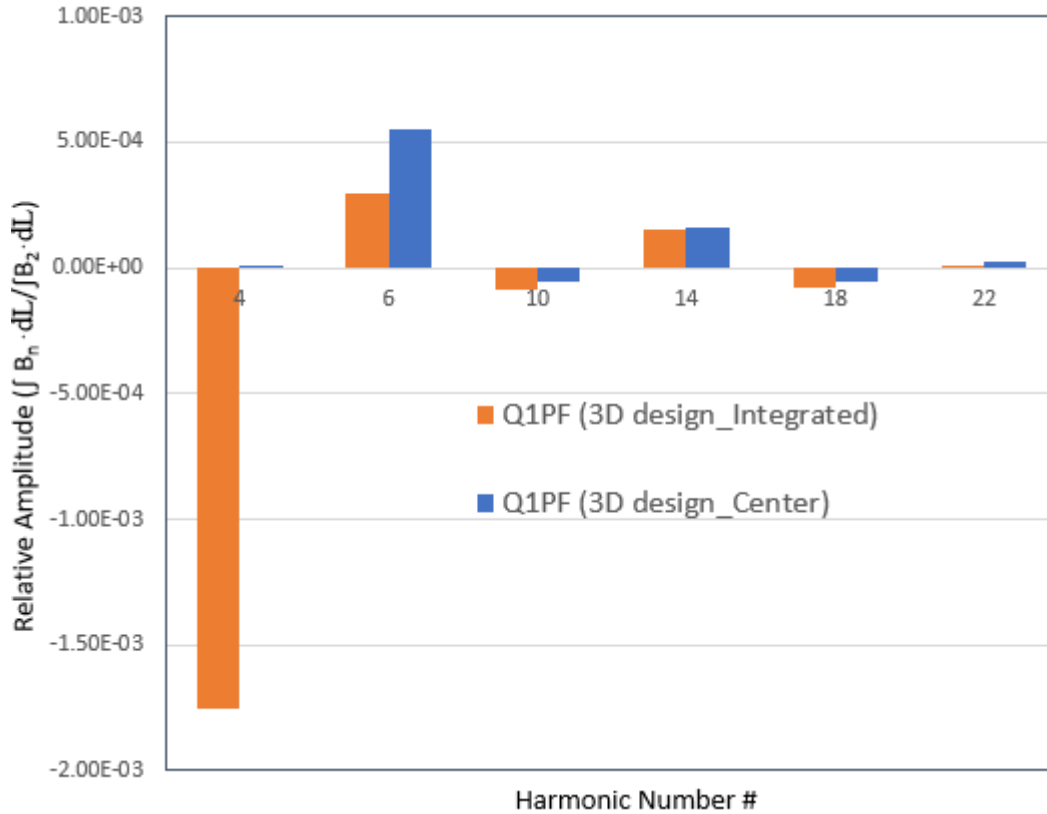


Figure 16: Relative amplitude of the integrated higher harmonics with respect to the integrated quadrupole component for 150 T/m field gradient of Q1PF quadrupole. Along with allowed quadrupole harmonics non-allowed octupole field component is present.

A full 3d model of the Q1PF along with the electron beam pipe is shown on the left side of Fig. 17. For symmetry purposes a cutout has been added in each quadrant. The location of the electron beam pipe is at 180 mm from the center of the magnet. The field profile along the electron beam axis is shown on the right side of the Fig. 17, where the calculated field value is around 0.3 Tesla. This field is too large and will need to be shielded. A cylindrical superconducting shield surrounding the electron beam is an option being considered [8]. The integrated strength of the field in the electron beam pipe located at 180 mm is required to be much smaller than the integral field strength (8.32 T·m) of the Q1PF. The calculated integral field strength along the electron path in the present design is 0.52 T·m.

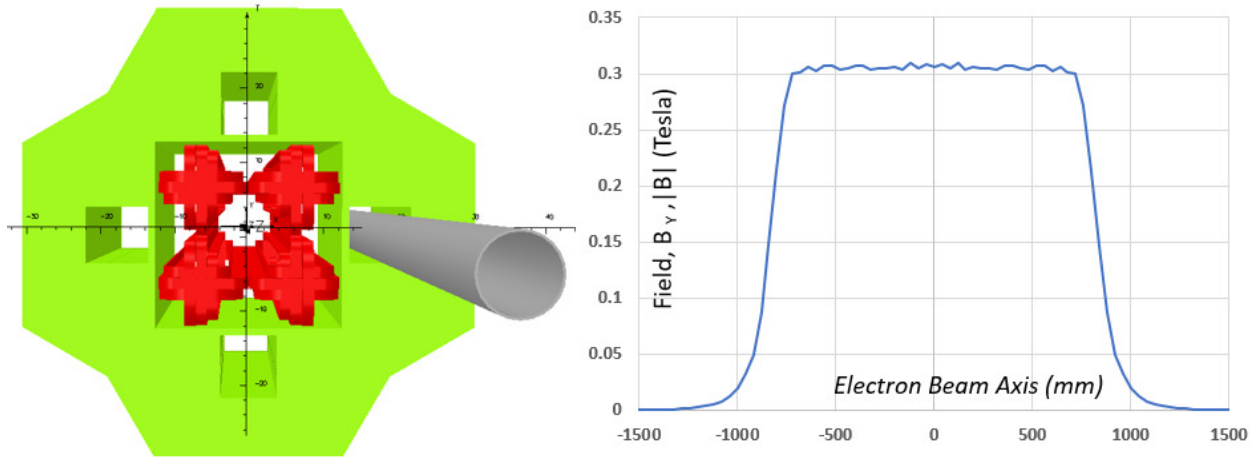


Figure 17: Full 3d model along with electron beam pipe at 180 mm from the magnetic center (on the left). Field plot along the electron beam axis (right). Units are in millimeter and tesla.

Forces for Symmetric Design

TOSCA was used to calculate the magnetic forces acting on the coils. For better understanding a 2d plot is overlapped over the coil-A and coil-B of the first quadrant. Based on the symmetry of the magnet system, each coil pack is divided into seven sections and each section has sub-sections along the beam axis (z-axis). For each section at full field, the net force vector magnitude and its orientation are obtained. The force vectors orientations and the corresponding magnitudes are provided in Table IX. The force vectors distributed over the corresponding sections were used for the structure analysis of the cold mass using the 2d FEA. It is important to note the coils are attracted to each other at the mid-plane. The resultant transverse force on each coil pack is outwards as shown in Fig. 19.

TABLE IX: Force Vectors Acting on the Sections of each Coil-Packs. Units are in kN

<i>Section</i>	Coil Pack A		Coil Pack B	
	F_x	F_y	F_x	F_y
<i>I</i>	62.1149	-37.2973	-38.5646	64.3112
<i>II</i>	1062.027	-13.4324	-16.1849	1192.9768
<i>III</i>	6.3197	-69.0176	-68.1797	69.0339
<i>IV</i>	59.44766	-73.8285	-74.3244	64.3956
<i>V</i>	-1355.45614	-281.6674	-276.6356	-1363.6656
<i>VI</i>	149.4928	-80.335	-80.9568	150.68761
<i>VII</i>	143.49224	-95.0351	-94.66503	144.79244
Total Force (kN)	184.315	-650.6132	-649.511	322.532

The calculated transverse forces towards the return yoke and the magnitude of the forces on the coil pack-A and coil pack-B are 184 kN and 323 kN, respectively, for each quadrant. This leads to an

unbalanced force towards the yoke side of around 140 kN in each quadrant due to different lengths of the two coil packs. The force vectors are shown in Fig. 19. The resultant vertical forces on each coil are around 650 kN; i.e., the coils are attracted to each other. For modeling purposes, we assumed a straight cutout in the return yoke. The impact of a cutout at an angle is not modeled nor analyzed.

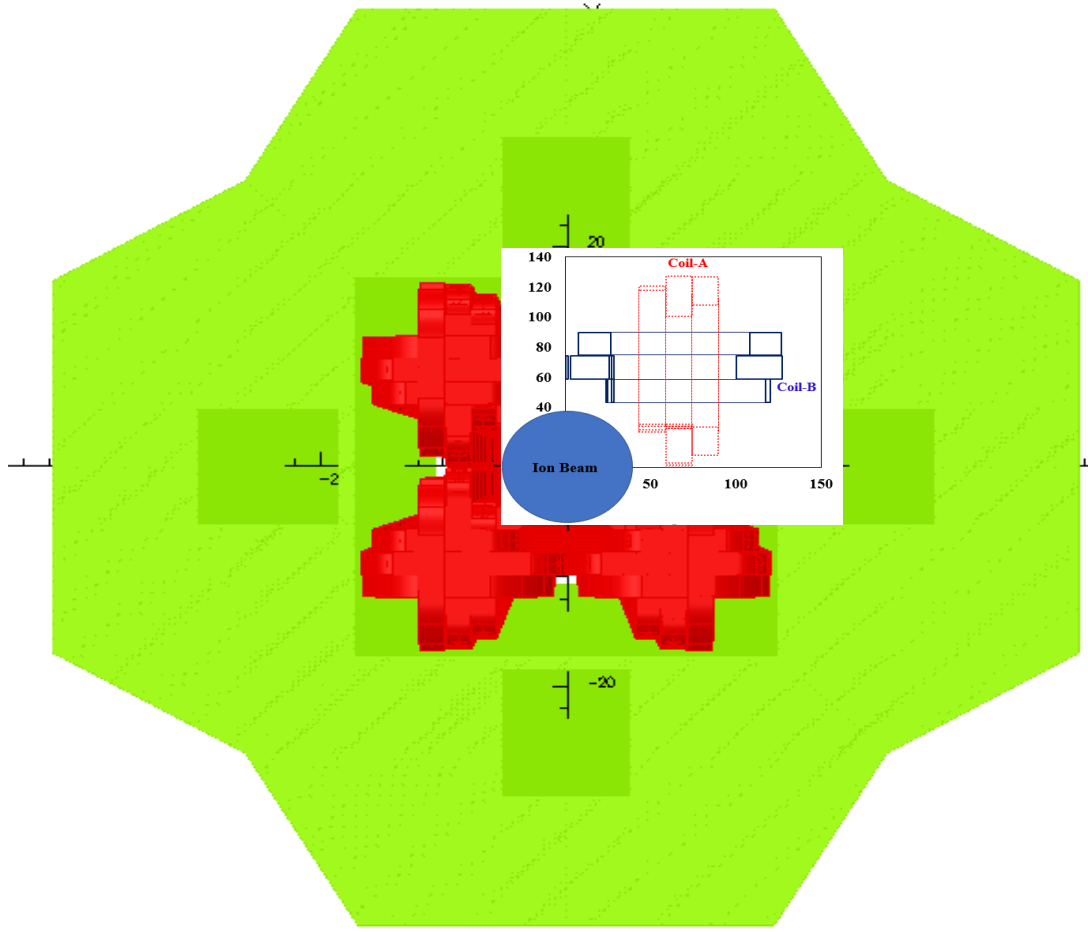


Figure 19: Decomposition of each coil-pack into seven sections and each section into sub-sections along the beam axis. See Table IX for details of the force vectors magnitudes and orientations.

The modular designs also offer a unique possibility to change the quadrupole apertures while using the same coil modules. We carried out a simulation where we moved the coil modules in the Q1PF magnet design to create the aperture for the Jefferson National Lab quadrupoles QFFB1_US, QFFB2_US, QFFB3_US designs and were able to obtain good field quality. As an example, in the model of the Q1PF without return yoke (Fig.20, left) coil modules are rearranged and moved towards the center by 10 mm to meet the requirements of JLAB QFFB1_US (Fig.20, right). The field contour on the surface of the Q1PF (left) and QFFB1_US (right) quadrupole conductor is shown in Fig. 21. Based on the 2d design a detailed analysis has been performed for the field quality and the results were compared. The field profile (B_y and B_{MOD}) along the mid-plane axis of the 2d analysis is shown in Fig. 22. The required engineering current density in QFFB1_US is about 85 % of Q1PF whereas the achieved field gradient is 5% higher. The modified model of QFFB1_US provides a field gradient of 148 T/m (2.96 T at 0.02m) and a peak field

in the straight section of the coil of 8.1 T. Other important design data such as magnitude of the higher harmonic components from the two quadrupole models are included in Table X.

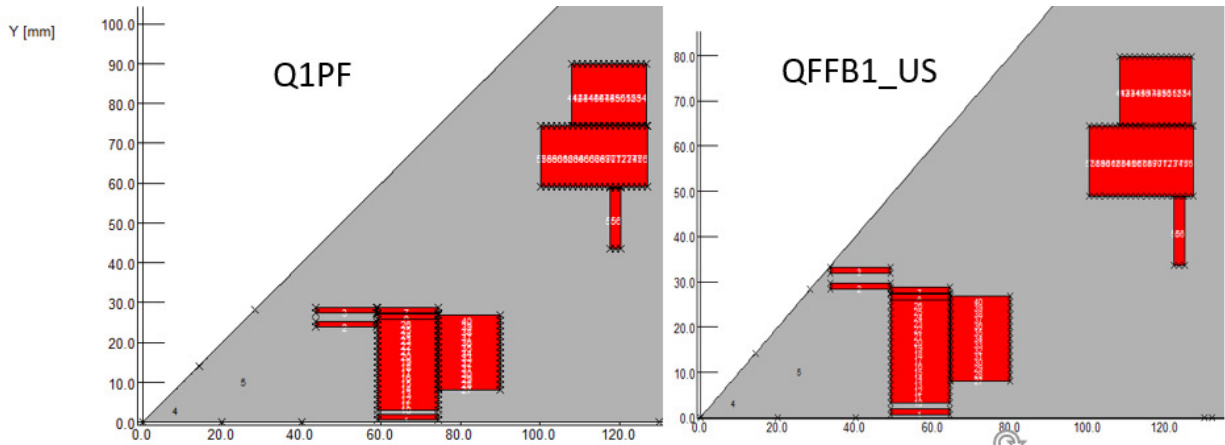


Figure 20: In the model of Q1PF (left) coil modules are rearranged and moved 10 mm inwards to satisfy the physical requirements of JLab’s QFFB1_US magnet (right).

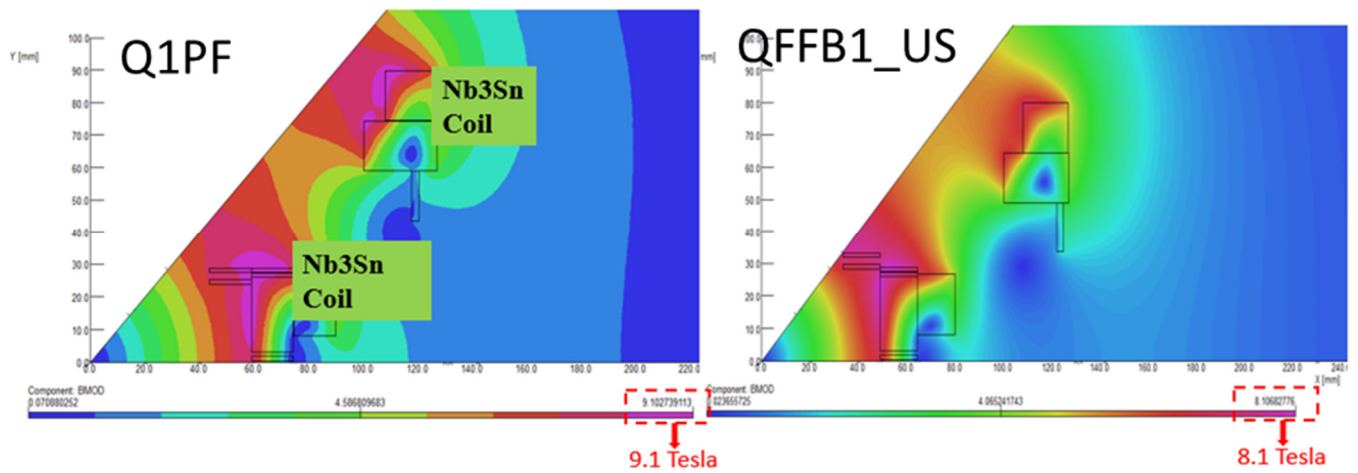


Fig.21. Field contour on the conductor surface of the Symmetric Q1PF and QFFB1_US designs. The peak field magnitude in the conductor is 9.1 T and 8.1 T respectively.

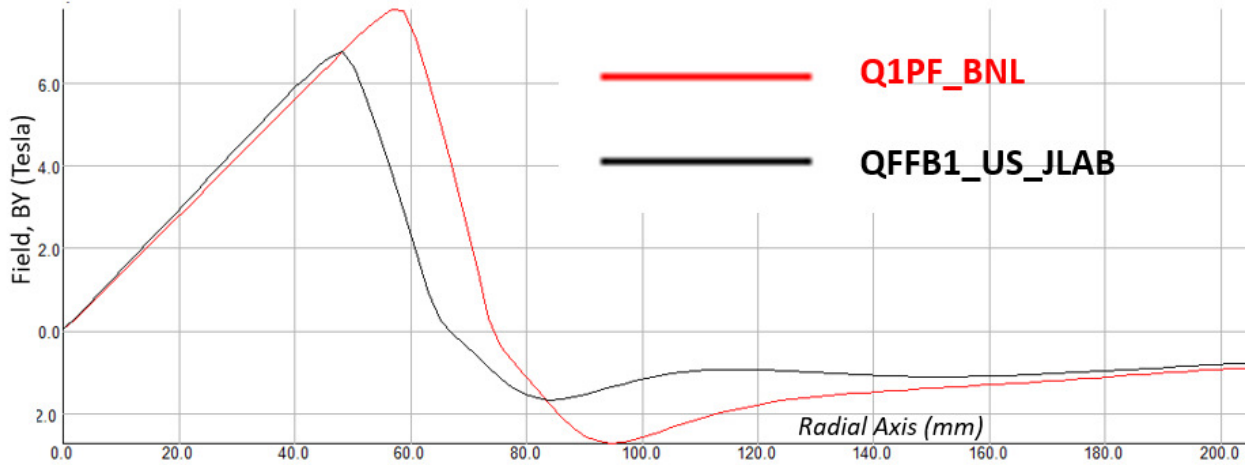


Figure 22a: Calculated field, B_Y (T) results from the 2d model compared along the radial axis. (Units are in millimeter and Tesla)

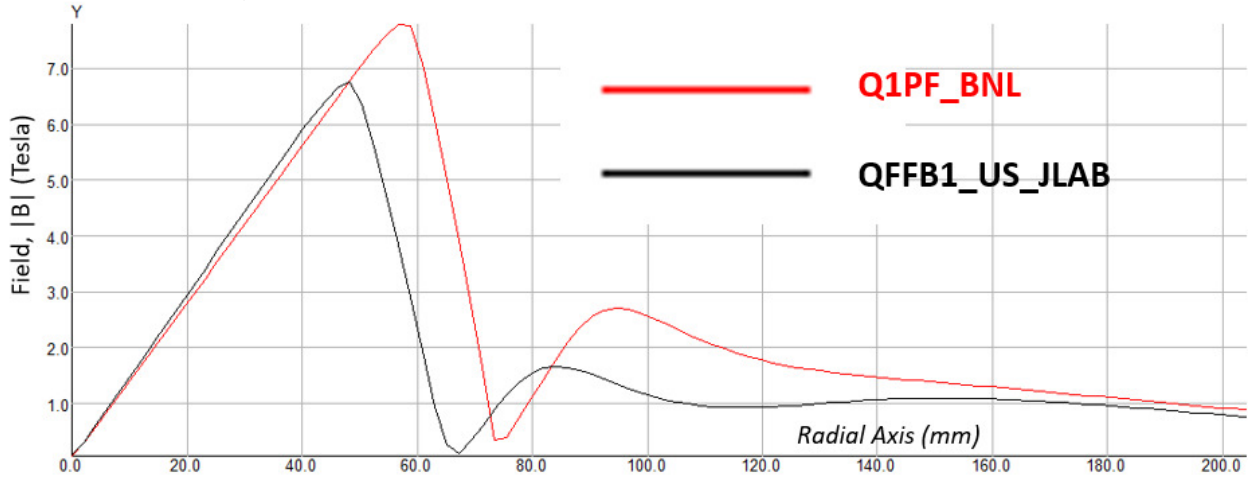


Figure 22b: Calculated field, B_{MOD} (T) results from the 2d model compared along the radial axis. (Units are in millimeter and Tesla)

TABLE X: Calculated Field Harmonics in the European Convention

Harmonic #	Q1PF (2D design)	QFFB1_US (2D design)
$B_2 \cdot dL$	--	--
b_6	$-3.14E-04$	$-5.24E-04$
b_{10}	$2.32E-04$	$2.47E-04$
b_{14}	$-2.23E-04$	$-2.25E-04$
b_{18}	$2.75E-04$	$2.76E-04$
b_{22}	$-1.75E-04$	$-1.75E-04$

Reference radius is 20 mm (75 % of the warm bore). $B_2 \cdot dL$ is integrated field strength in T·m. The other components relative to the quadrupole field value in the center.

SECTION C: ASYMMETRIC MAGNET 2D AND 3D DESIGN WITH OPERA

An alternate approach that we investigated was the *simpler* design. Rather than split the return of the current to both sides of the magnet, the simpler design returns all the current on one side (the right side in the figures shown). The *simpler* design is simpler to assemble but does not have standard quadrupole boundary conditions (symmetry) and consequently there are non-allowed skew harmonics present. This can be addressed by rotating the magnet during installation as we shall discuss. Also the design requires more space to contain the part of the coils returning the current, thus making the magnets wider. The mass of the yoke and cross-section of the superconducting coil were optimized within constraints while keeping field quality over the operating range. The optimized cross-section of the BNL Q1PF is shown in Fig. 23. The figure shows one quadrant with the periodic boundary conditions that flips the sign of the vector potential A_z at 90° with respect to A_z at 0° .

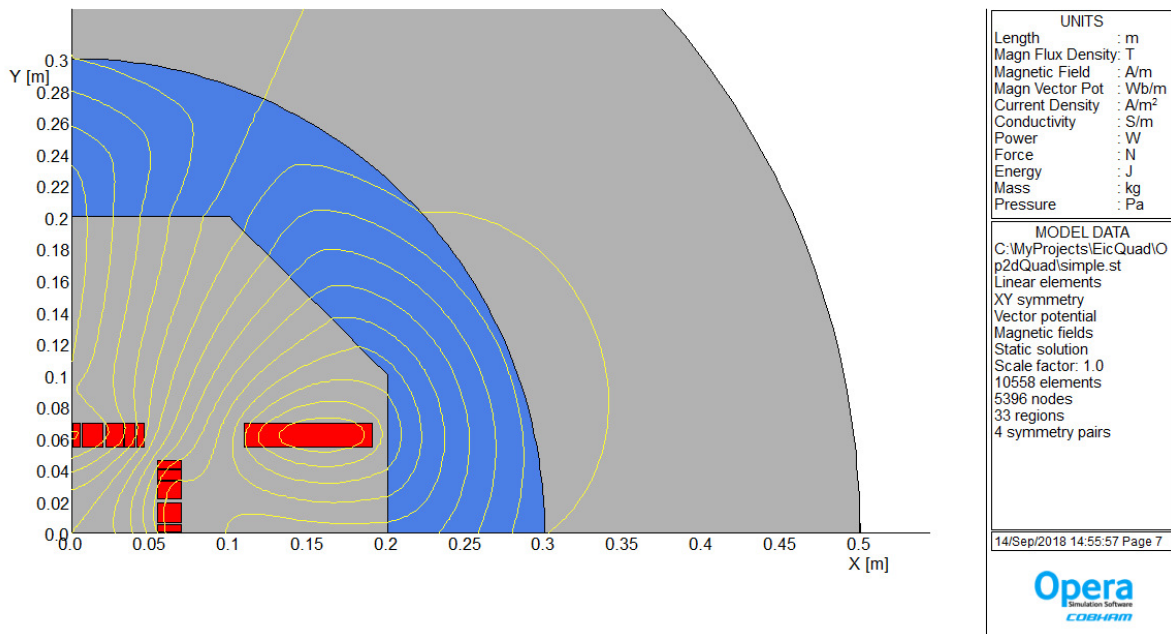


Fig.23. OPERA2d of the *simpler* modular design with flux lines. The figure shows a quarter model with periodic anti-symmetric boundary conditions. The location of the electron beam center is below the return coil block and is at 0.18 m from the magnetic center.

Fig. 24 shows an OPERA2d field contour plot for the Q1PF quadrupole design. The peak field magnitude in the coil is around 11.5 Tesla whereas the peak magnitude of the field in the iron is around 5.96 tesla. It also shows the field magnitude in the region of the electron beam pipe. The yoke cross-section is also optimized to meet the physical constraints around the magnet. The Q1PF quadrupole model provides a field gradient of 140 T/m and a peak field at the pole ($r = 0.036$ m) of 5.05 T.

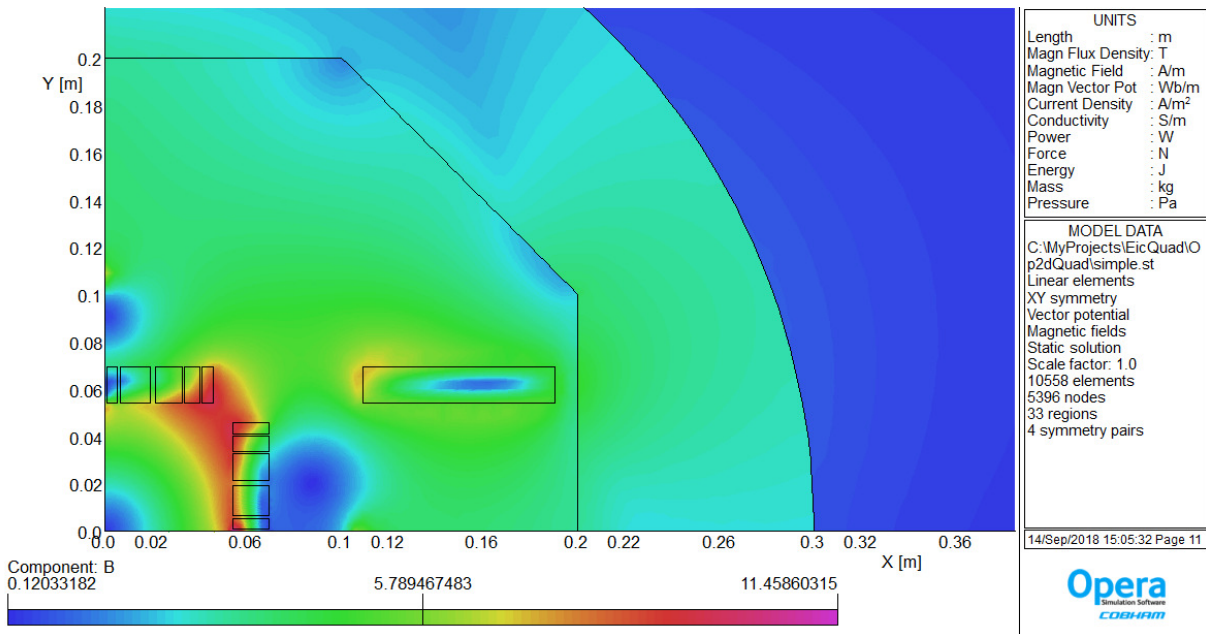


Fig.24. Field contour on the surface of the *Simpler* Q1PF quadrupole design. The peak field magnitude in the conductor is around 11.5 Tesla.

Based on the 2d optimized design, 3d modeling was performed. The 3D model provides an opportunity to examine the magnet in detail, especially the flux distribution along the ion/proton beam region, the stray field in and along the electron beam pipe, the peak field in the coil area, the integrated higher harmonic contents, and the forces on the coil, a magnetic model has been developed. Fig. 25a shows the 3D meshed model of the BNL_Q1PF quadrupole with coils and the surrounding air region. There are a total of four coils and the advantage of this design over the *Symmetric* modular design is that there is no interference between coils at the ends. Fig. 25b shows an OPERA3d field contour plot for the Q1PF quadrupole design. The field on the coil surface is shown in Fig. 26. The peak field on the coil from the 3D program is 11 T which occurs where the two neighboring coils are closest. The field components, B_y and B_x profile along the mid-plane axis are shown in Fig. 27. Because the mid-plane axis is not a quadrupole symmetry axis for the simpler model the B_x component does not vanish. The field in the region around 0.175 m where the electron beam is located has a value ~ 3.5 T. The field value in the region of the electron beam is significantly high and additional approaches will be needed to shield the electron beam from the field. BNL/PBL has a separate grant to investigate using HTS to shield magnetic field [5]. The saturation of the iron in the return yoke leads to significant field outside the iron. The field just outside of the yoke as a function of angle is shown in Fig. 28. The calculated peak field is 0.8 T at $\sim 20^\circ$.

Fig. 29a shows the relative amplitude of higher harmonics in the center of the *Simpler* Q1PF quadrupole from the 2d and 3d model analysis. The harmonics were analyzed at each excitation current of the magnet. To limit the large value of the b_6 and b_{10} over the operating range of the large field gradient quadrupole (Q1PF) coil optimization has been performed. The optimization of the 2d model achieved values for the *allowed* higher harmonics that are within the design specification but the magnitude of the *non-allowed skew* quadrupole component is around 18% relative to the *normal*

quadrupole field. We will show that the skew harmonics can be eliminated by rotating the magnet during installation. The values of the first few allowed and non-allowed higher harmonics in the center of the magnet at peak operating field are given in Table XI. The data extracted from the 3d model is used for integrated harmonic analysis. The values of the first few allowed integrated higher harmonics and integral field strengths at maximum field are given in Table XII. Along with the allowed harmonics of quadrupole field such as b_6 , b_{10} , $b_{14}\dots$, $b_{(2n+2)}$, non-allowed a_6 , a_{10} , $a_{14}\dots$, $a_{(2n+2)}$, are present. The relative amplitudes of the higher harmonics (integrated and in the center) with respect to the quadrupole component are shown in Fig. 29b.

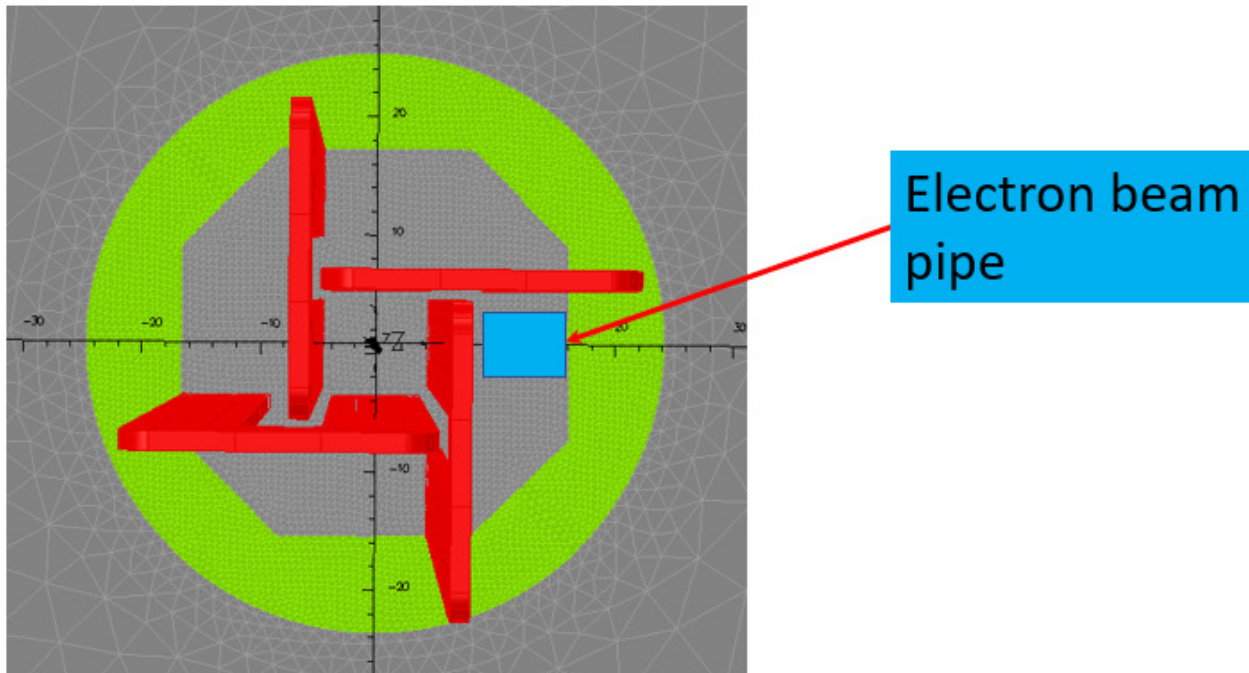


Fig.25a. 3d meshed model for *simpler* superconducting Q1PF quadrupole magnet with coils, return yoke and background air.

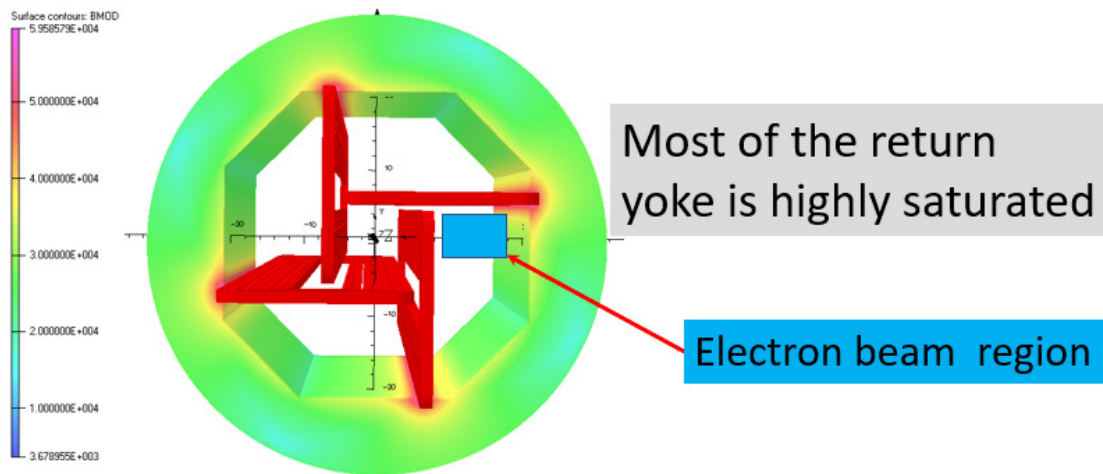


Fig.25b. OPERA3d model with the field contour on the surface of the return yoke. The blue rectangle below the return coil block is for the electron beam pipe.

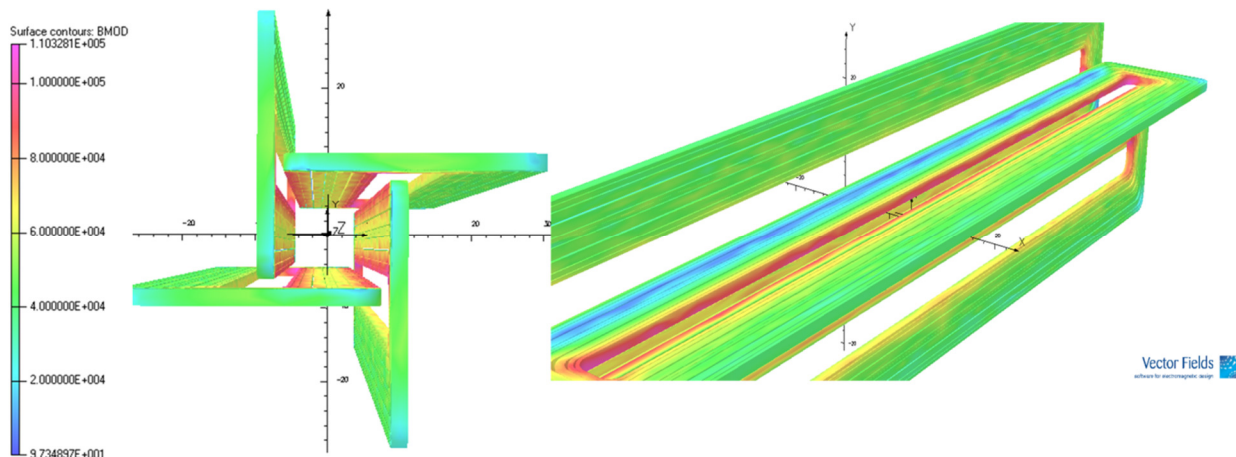


Fig. 26: The 3D analysis provides the $|B|$ on the surface of the simpler design coils. The peak field occurs where neighboring coils are closest.

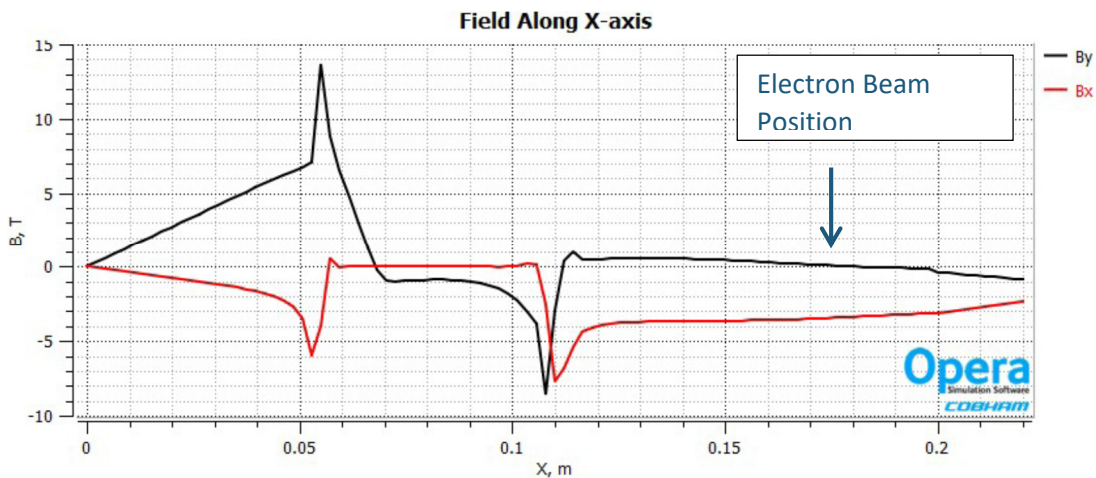


Fig. 27. B_y and B_x calculated along the mid-plane axis from the 2d model. (Units are in meter and Tesla).

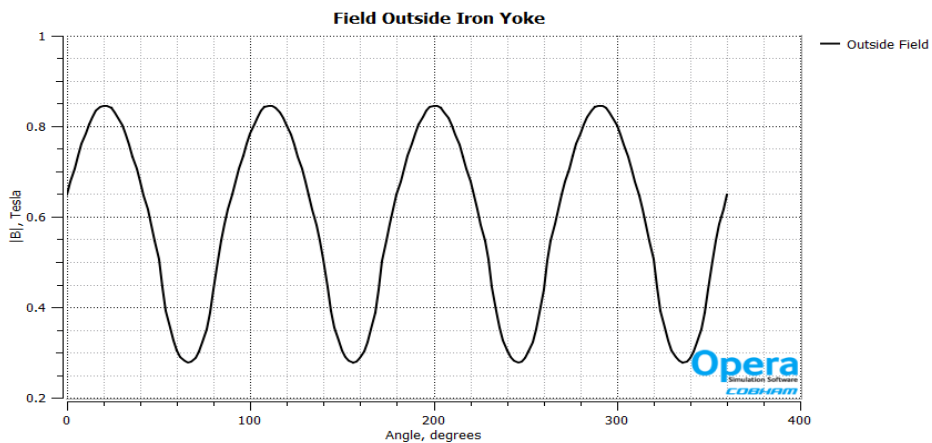


Fig. 28: $|B|$ just outside the yoke. The figure shows field that punches through the iron.

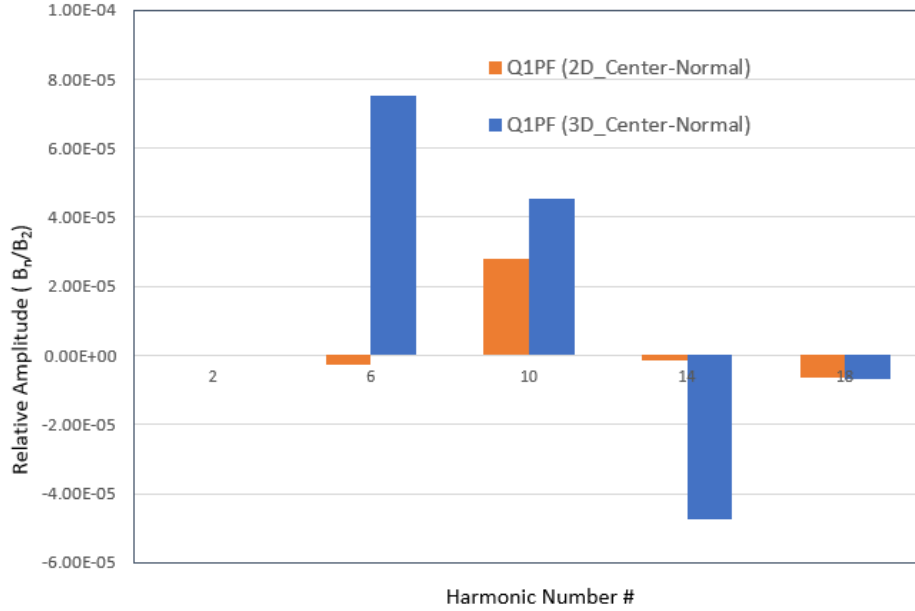


Fig. 29a: Relative amplitude of the higher harmonics with respect to the quadrupole component for 140 T/m field gradient of Q1PF *Simpler* quadrupole. The 2D harmonics are from Opera2D and the 3D harmonics are calculated with Tosca at the axial center of the magnet.

TABLE XI: Comparison of Harmonics for Q1PF Calculated for 2D with 3D Harmonics Calculated at Axial Center of the Magnet

Harmonic#	Q1PF (2D design)		Q1PF (3D design)	
	Normal (B_n/B_2)	Skew (A_n/B_2)	Normal (B_n/B_2)	Skew (A_n/B_2)
b_2, a_2	1.0	-1786E-04	1.0	-1713E-04
b_6, a_6	-0.026E-04	-0.86E-04	0.754E-04	-0.49E-04
b_{10}, a_{10}	0.281E-04	-0.15E-04	0.455E-04	-0.23E-04
b_{14}, a_{14}	-0.016E-04	0.026E-04	-0.474E-04	0.018E-04
b_{18}, a_{18}	-0.064E-04	0.008E-04	-0.068E-04	0.14E-04

Reference radius is 36 mm (75% of the warm bore). The other components relative to the quadrupole field value in the center.

Figure 30 shows the normal (blue) and skew (red) quadrupole (left) and duo-decapole (un-normalized B_6 and A_6) (right) harmonics as a function of axial position measured from the magnet center. The harmonics are calculated at each axial location by a Fourier transform of B_r on a circle with radius 36 mm. These harmonics are calculated from the coils alone without iron included. The harmonics vary rapidly in the magnet end region. This explains the differences of the integrated and center harmonics.

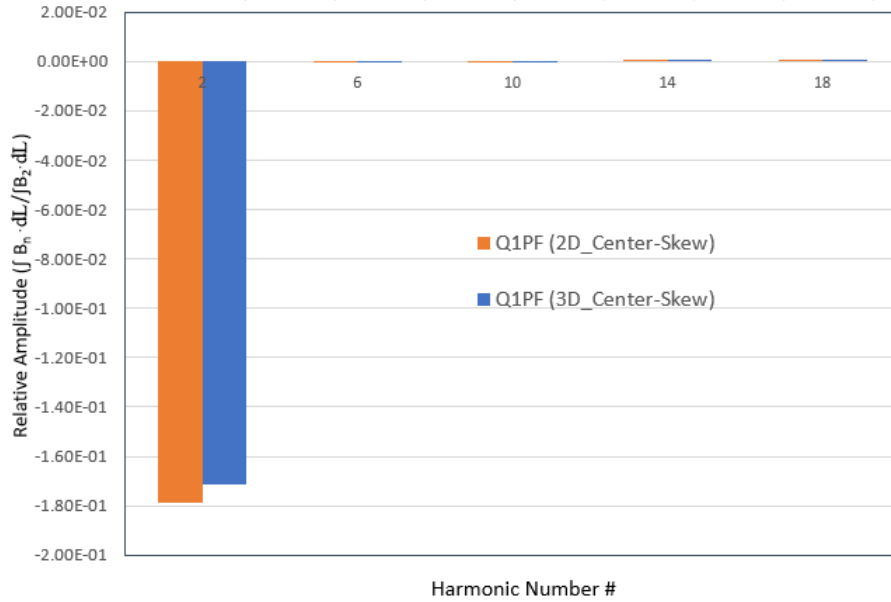


Fig.29b: Relative amplitude of the integrated higher harmonics with respect to the integrated quadrupole component for 140 T/m field gradient of Q1PF quadrupole. Along with allowed quadrupole harmonics non-allowed components are present.

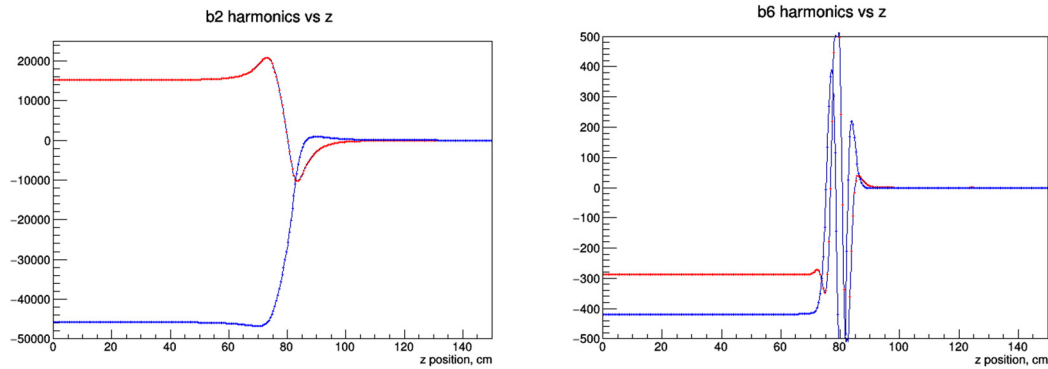


Fig. 30: Left: Normal (blue) and Skew (red) quadrupole harmonic as a function of axial position measured from the magnet center. Right: Normal (blue) and skew (red) duo-decapole harmonic as a function of axial position.

TABLE XII: Calculated Integrated Field Harmonics in the European Convention

Harmonic order	Q1PF (3D design) <i>Normal</i> (B_n / B_2)	Q1PF (3D design) <i>Skew</i> (A_n / B_2)
b_2, a_2	1.0	-1865E-04
b_6, a_6	-1.54E-04	-11.2E-04
b_{10}, a_{10}	0.325E-04	-0.43E-04
b_{14}, a_{14}	0.055E-04	-0.13E-04
b_{18}, a_{18}	-0.035E-04	-0.54E-04

Reference radius is 36 mm (75%) of the warm bore. The other components are relative to the quadrupole field value in the center.

Forces for the Simple Design

Coil-A			Coil-B			Coil-C			Coil-D		
Section #	$F_x(N)$	$F_y(N)$	Section #	$F_x(N)$	$F_y(N)$	Section #	$F_x(N)$	$F_y(N)$	Section #	$F_x(N)$	$F_y(N)$
1	150091	143563		157213	-142957.33		-148695.1	-151440		-142287	150323
2	189130	186339		187558	-190732.61		-197332.1	-185650		-186252	195701
3	352854	277896		266604	-354924.4		-349613.3	-278163		-277530	353526
4	462812	185019		183231	-468563.39		-457448.9	-183072		-187523	481465
5	188046	26150		29024	-210946.27		-189017.5	-23860		-25553	196423
6	211857	13244		16319	-210946.27		-202527.2	-18006		-15878	206108
7	663740	-68320		-59422	-653099.04		-659175.7	57571.3		59388	656410
8	725294	-202122		-195422	-729907.23		-719613.6	191608		182901	723843
9	484293	-168421		-162006	-472675.18		-483688.8	167507		164302	487365
10	397328	-146083		-139037	-400207.52		-397379.6	131616		145216	393217
Total Force (N)	3825445	247265		284062	-3818320.2		-3804492	-291890		-283214	3844379

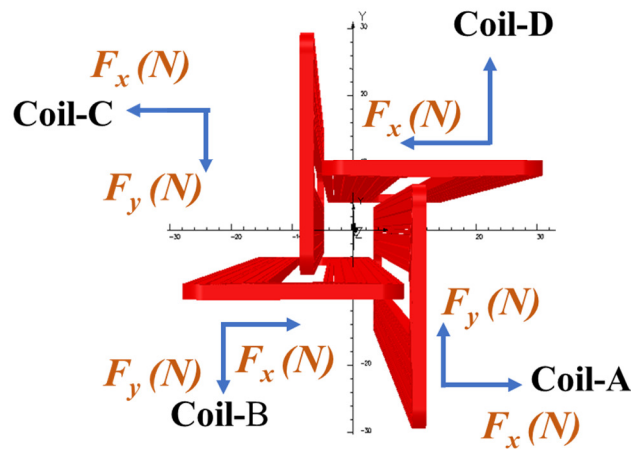


Table XIII: Forces on Simpler Design Coils in Newtons

Table XIII shows the Lorentz forces for the simpler design as calculated by Tosca. The section numbers correspond to the different blocks in each coil. Since all of the coils are identical the forces for the four coils sum to zero. The discrepancies are an indication of the size of the computation errors. One does expect that there should be a non-zero torque. The axial torque is $\tau_z = -61183$ kN-m. This torque would be transferred to the return yoke, which must be secured to external support. This will affect the cryostat design.

SECTION D: SIMPLER MODEL CALCULATED WITH ROXIE

Table II and Table III show a configuration D which describes a single layer coil with the simpler geometry with the current returned on one side rather than split between the two sides. Otherwise the coil configuration is similar to the symmetric configuration C. As Table III shows it also has a similar quench margin where the operating current is 89% of the quench current. A double layer coil would have a larger margin.

Table XI and Table XII show a large skew quadrupole (a_2) term. The skew quadrupole term can be zeroed by rotating the magnet during installation. The angle of rotation is determined by zeroing the rotated a_2' (rotated harmonics are primed). The rotation angle to zero a_2' is -5.076° . Figure 31 shows the rotated magnet that zeros the skew harmonics. The figure also shows $|B|$ in the iron with a maximum field in the vicinity of the return coil. The iron saturation pattern does affect the rotation angle by $\sim 0.5^\circ$. Rotating the magnet to eliminate the skew quadrupole does not necessarily eliminate the higher allowed harmonics, since the rotated angle for each harmonic is multiplied by the harmonic

order. To minimize the higher order skew harmonics the magnitude of that harmonic, $\sqrt{b_n^2 + a_n^2}$, must be minimized. We have used the *Roxie* program [7] to optimize and minimize the duo-decapole harmonics (b_6, a_6) by varying the gaps between the coil blocks. Table XIV shows the resultant rotated harmonics. The optimized duo-decapole harmonics are negligible. The next higher allowed harmonics (b_{10}, a_{10}) were not explicitly included in the minimization fit, however the b_{10}' and a_{10}' harmonics are quite acceptable.

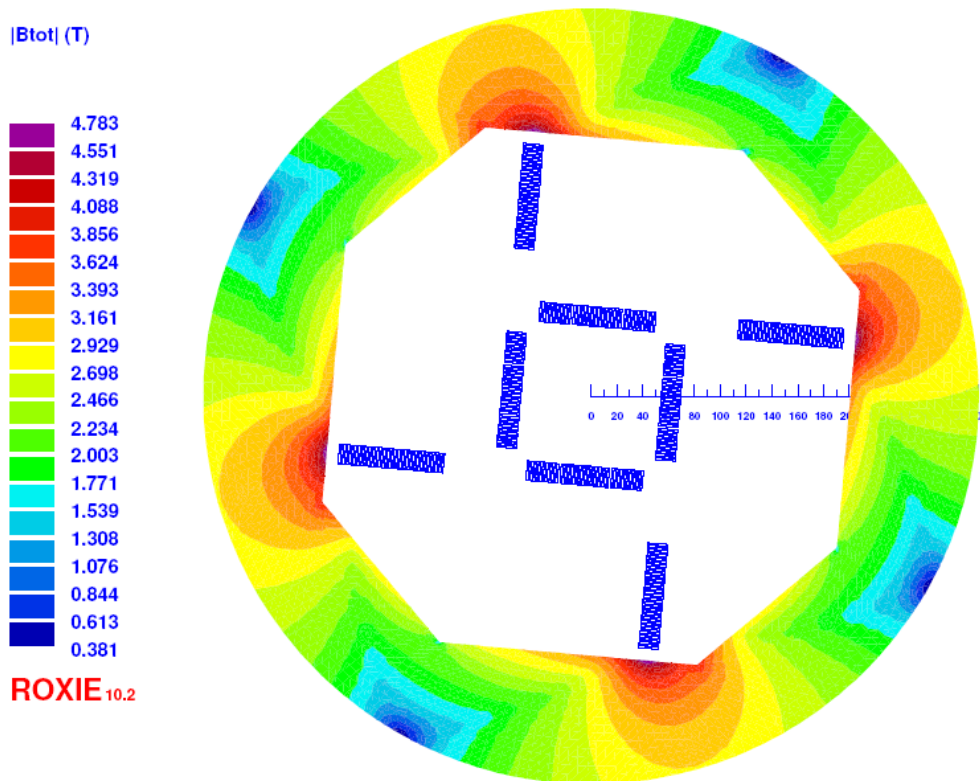


Fig. 31: Rotated simpler quadrupole. The magnet is rotated by -5.076° to zero the a_2' harmonic.

Table XIV: Optimized Rotated Harmonics for the Simpler Quadrupole

Order	Normal b_n	Skew a_n	Normal b_n'	Skew a_n'
			Rotated	Rotated
2	10000	-1561.86	10000	-0.16669
6	-0.02287	-0.77642	0.00084	0.0001
10	0.28870	-0.15468	0.25315	0.23133
14	-0.01696	0.02706	-0.04202	0.00959
18	-0.06562	0.00872	-0.01032	-0.06104

SECTION E: MECHANICAL DESIGN ANALYSIS

A structural analysis of the *simpler* design (design D) and the *symmetric* design (design A) were performed using the ANSYS 2d finite element program. For the analysis we have assumed that coils are held in place with a stainless steel 304 collar that has a 96 mm aperture hole for the beam. The mechanical analysis for the *simpler* and *symmetric* designs is given in the subsections.

Simpler Design

The procedure was to use ANSYS to calculate the field (and compare it to OPERA) to obtain the Lorentz forces locally at each node. Because the simpler design does not satisfy the normal quadrupole mirror symmetry, an anti-symmetric 90° rotational boundary condition was used for the magnetic simulation. (A boundary condition on the vector potential, $A_z(0^\circ) = -A_z(90^\circ)$ was imposed.) Because the Lorentz forces are proportional to both J and B , the mechanical displacements show a 90° rotational symmetry. Figure 32 shows a $|B|$ field contour plot from ANSYS that can be compared to figure 19 from Opera2d. The ANSYS plot shows a peak field of 10.3 T which is slightly lower than the Opera2d value (11.5 T) but occurs at the same location near the coils. The differences may be due to different BH tables used by the two programs. These differences are not important for the structural calculation. ANSYS will use the same mesh geometry for the magnetic calculation as for the structural analysis. Figure 33 shows the contour of A_z which illustrates the magnetic flux lines. Examining the lines at the borders shows the effect of the anti-symmetric 90° periodicity. The flux lines in the interior of the coils show quadrupole symmetry.

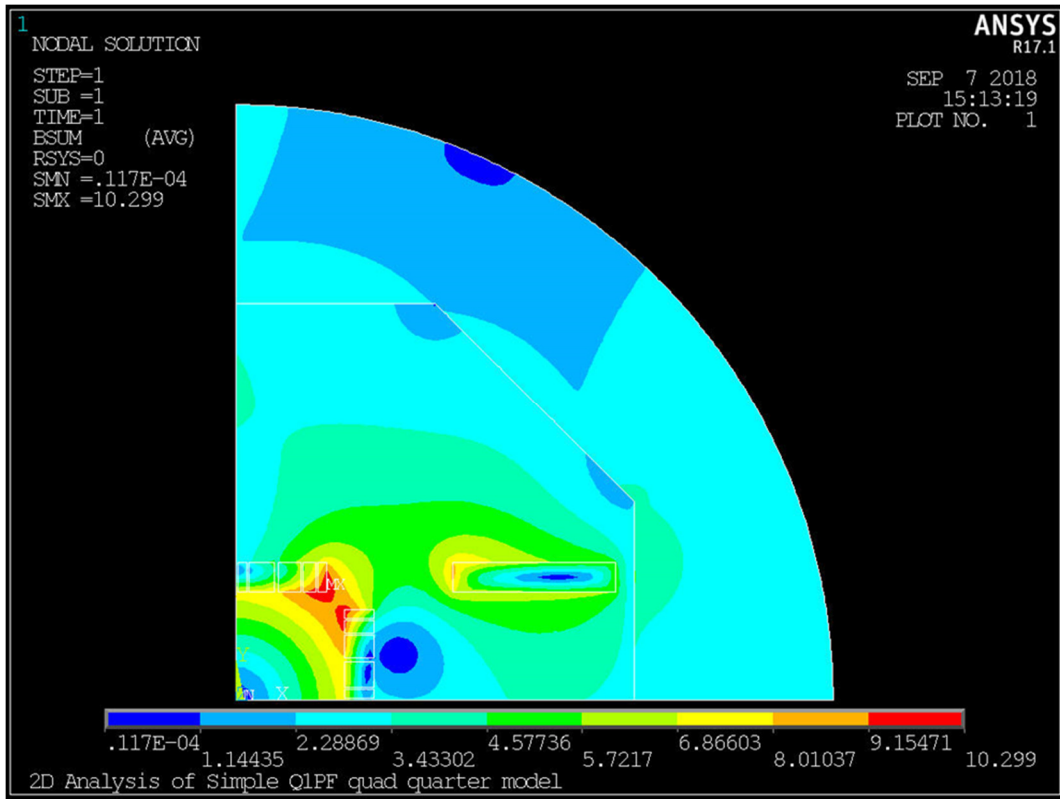


Fig. 32: Contour plot of $|B|$ calculated by ANSYS.

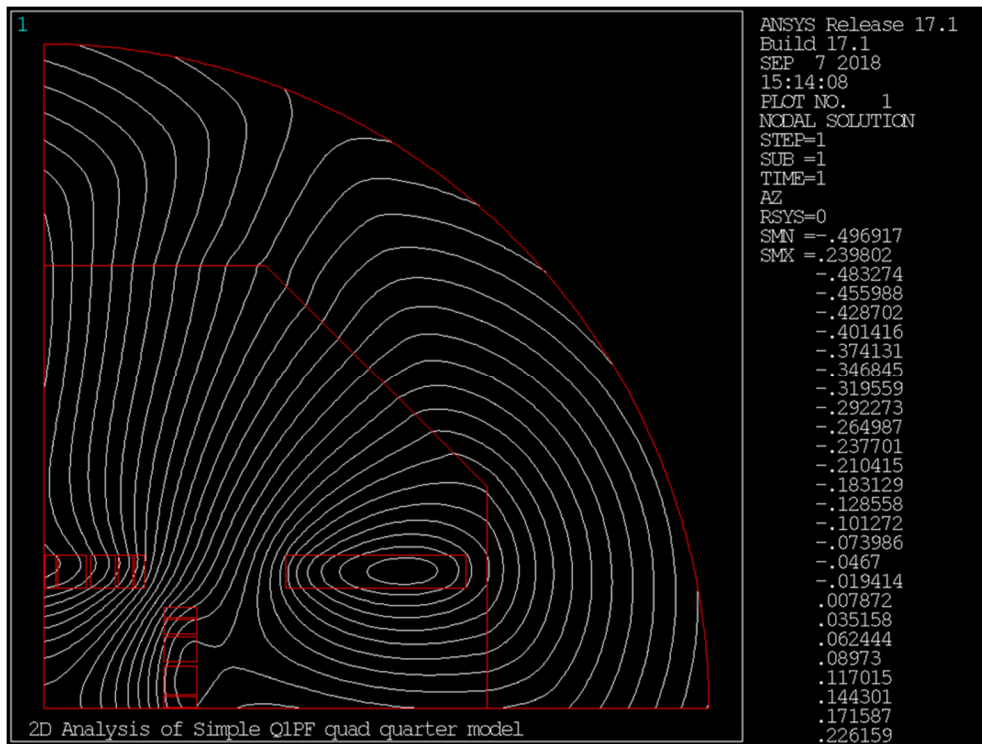


Fig 33: Contour plot of A_z from ANSYS calculation which shows the magnetic flux lines.

For the structural analysis some assumptions about the materials need to be made. The elastic modulus of Nb₃Sn conductor is dependent on whether it is wind-and-react or react-and-wind. Also the coils will be epoxy impregnated which softens the modulus. The modulus largely affects the strain calculation which is important since Nb₃Sn has a low strain limit. In our calculations we used a Young's modulus of 44 GPa for the Nb₃Sn coils and assumed that the modulus was isotropic [8]. Figure 34 shows a plot of the nodal displacements. The plot on the left superimposes the distorted magnet (blue) onto the undistorted. The plot on the right presents the displacements as a contour plot. The maximum displacement observed is 10.5 μm and occurs at the coil mid-planes. As mentioned the distortions in the coil are dependent on the modulus used. Figure 35 shows an enlarged view of the displacements in the coils. The collars will need to supply pre-stress to suppress coil movement as the magnet is ramped up. Applying pre-stress for racetrack coils is one-dimensional making it simpler than for cos(2-theta) magnets.

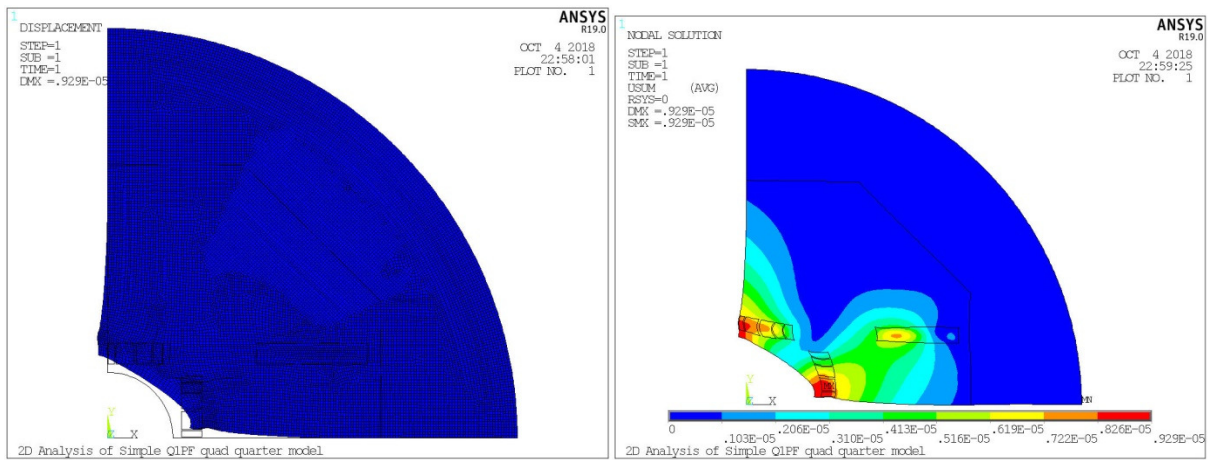


Fig. 34: Nodal displacements of the simpler design model. Left: Comparison of distorted model to the undistorted. Right: Contour plot of nodal displacements.

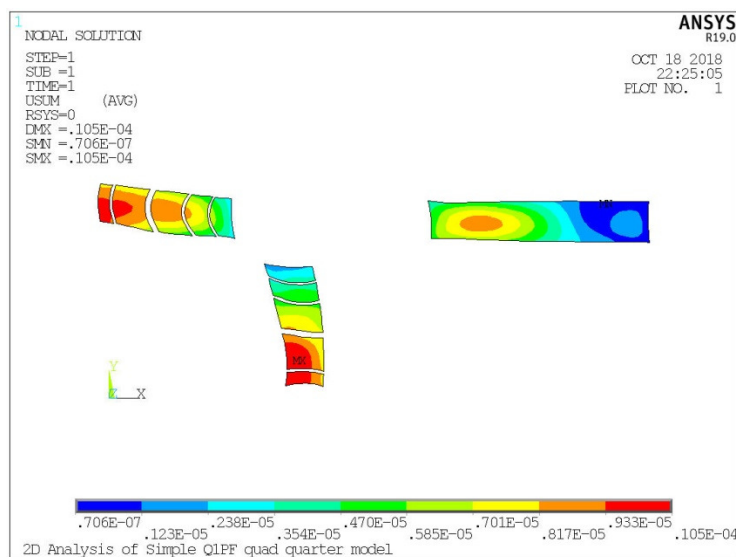


Fig. 35: Contour plot of coil displacements. The distortions are exaggerated.

Figure 36 shows the von Mises stress for the simpler design. The peak stress occurs in the collar on the web between the coils. There is also a bending stress that occurs on the inner surface of the aperture. The peak stress is sufficiently below the limiting values for the materials. Figure 37 shows the strain associated to the von Mises stress.

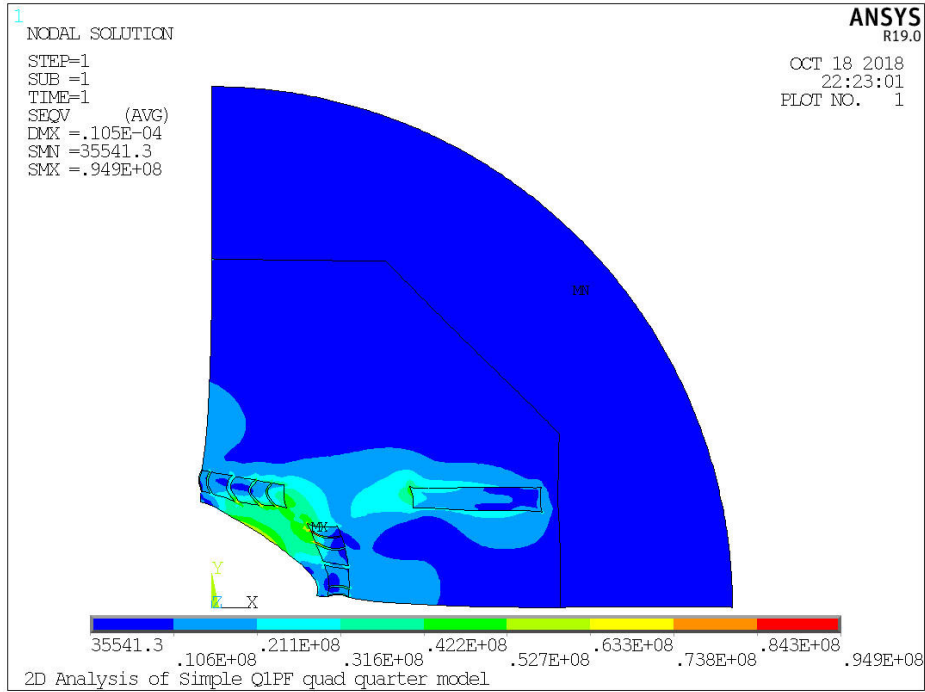


Fig. 36: Contour Plot of the von Mises stress for the simpler design. Stress units are pascal.

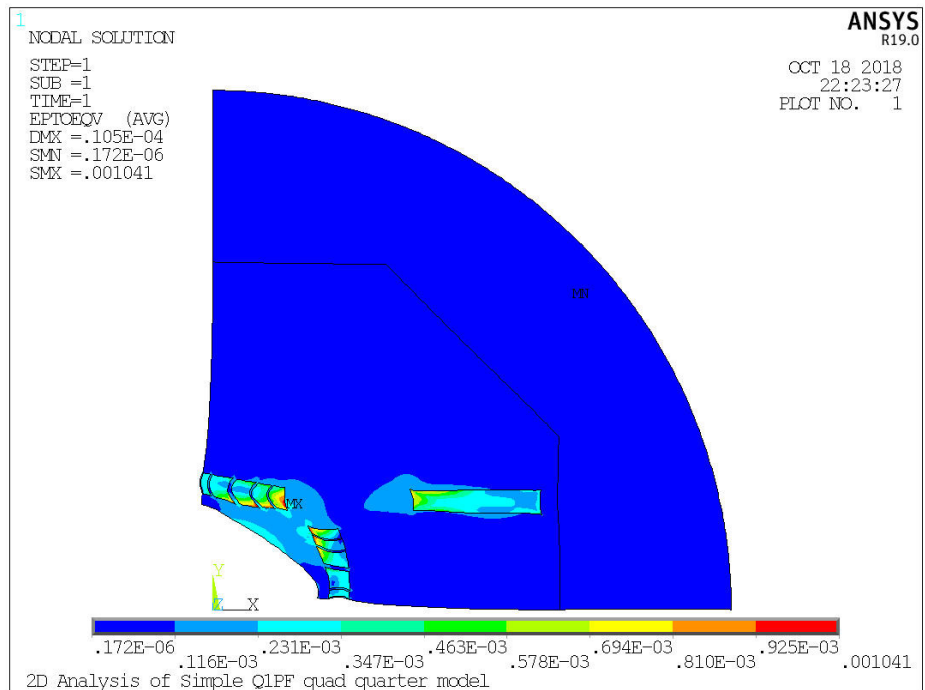


Fig. 37 Contour plot of the strain associated to the von Mises stress.

Figure 38 shows the von Mises strain in the coils. Nb₃Sn conductor can be degraded if the strain reaches the irreversible limit. The maximum strain in the coils for the simpler design is 0.1% which is sufficiently below the acceptable limit. Column 2 in Table XV summarizes the peak values for this design. The limiting values are listed in column 4 of the same table.

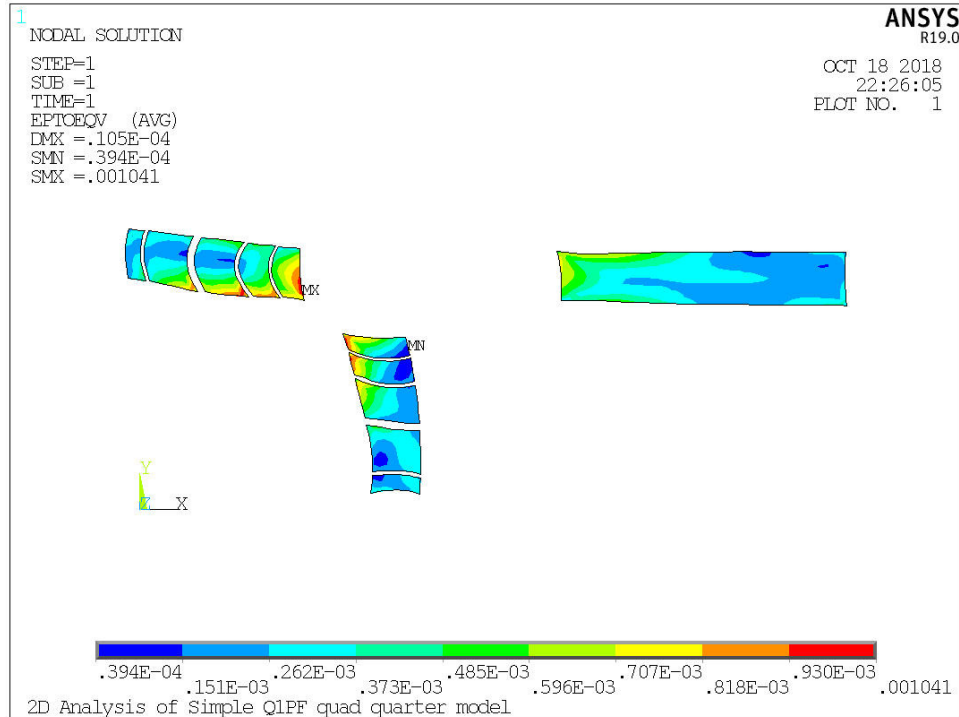


Fig. 38: Von Mises strain in the coils for the simpler model.

We have used a Young’s modulus of 44 GPa for the Nb₃Sn conductor in order to calculate the strain on the conductor from the Lorentz forces. Table XIV summarizes the peak values for this design in column 2. The limiting material values are shown for comparison.

Assembly of the Simpler Design Magnet

An important engineering issue is how to assemble the simpler magnet. Fig. 39 shows a 2D sketch of the assembled magnet. The design uses four double racetrack coils. Each single coil is wound onto a stainless-steel form and mated to the second coil. The inner coil lead splice is located inside the support form. The arrangement simplifies the lead design and has been used previously at BNL. Instead of using interlocking keyed collar laminations, the coil supports are a series of solid stainless-steel bars that run the full length of the coil, offering the same radial and azimuthal support to the coil ends as well as their straight section. The bars are screwed together through holes in the coil forms. Inner support is offered by the square bore center insert while coil axial torque is restrained by the octagonal inner surfaces of the steel yoke. The coil assembly is expected to be a precision running fit against the yoke, thereby offering additional radial support to the coils as well as permitting their complete removal from either end.

Coil replacement is a simple matter of disassembly involving no pressing, un-keying, or cutting. Coil sets of different dimensions would be accommodated by a different set of support bars dimensioned

appropriately. The four large voids inside the iron provide space for four stainless steel tie-rods which along with a pair of end plates, provide restraint against axial Lorentz forces.

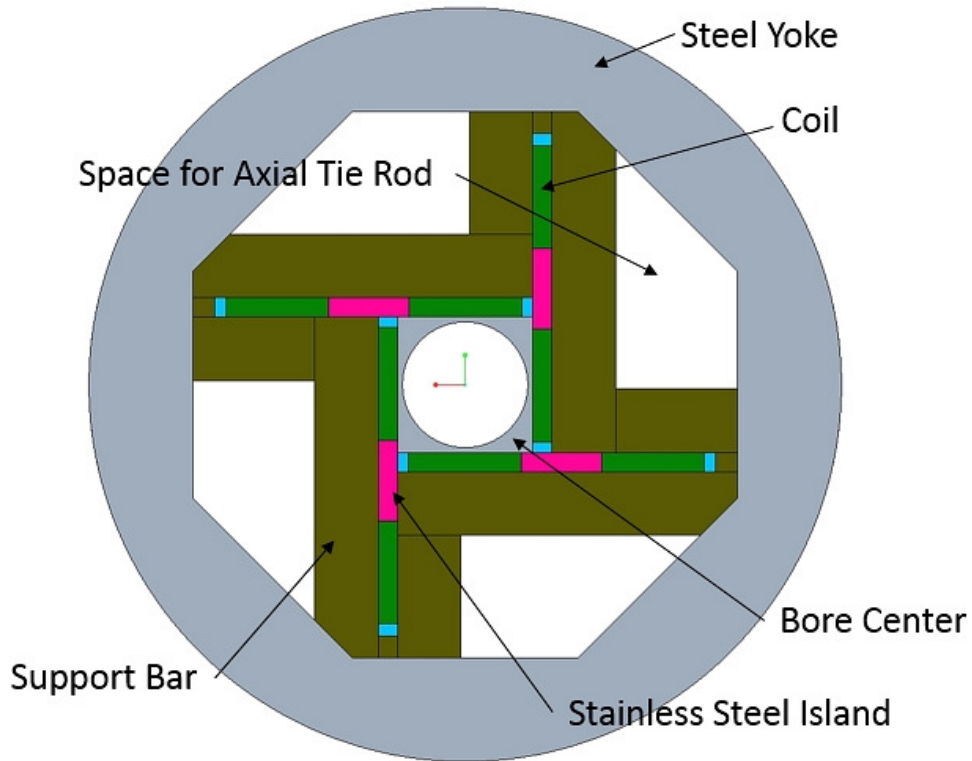


Figure 39: Sketch of the collaring support structure for the simpler magnet design.

Finite element analysis was performed on the 2D cross-section using ANSYS Maxwell to generate the Lorentz forces at full power (140 T/m). Flux and field plots are shown in Figures 40.

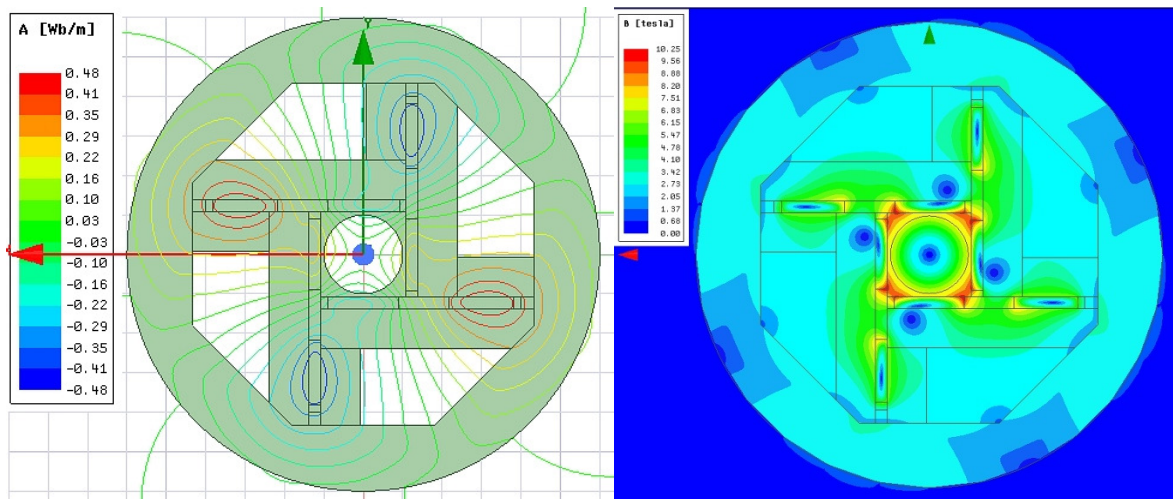


Figure 40: Flux (left) and |B| plot [right] for the simpler magnet with the stainless steel bar support.

The structural analysis is preliminary and conservative at the time of this writing. However the results so far are encouraging. Figure 41 shows the x-component of the normal stress and strain on the coils which shows the compression of the coil conductors. The coil stresses and coil strains are manageable and do not exceed 0.21%. Stresses in the support structure including the yoke do not exceed 93 MPa and deflections are small (Figures 42).

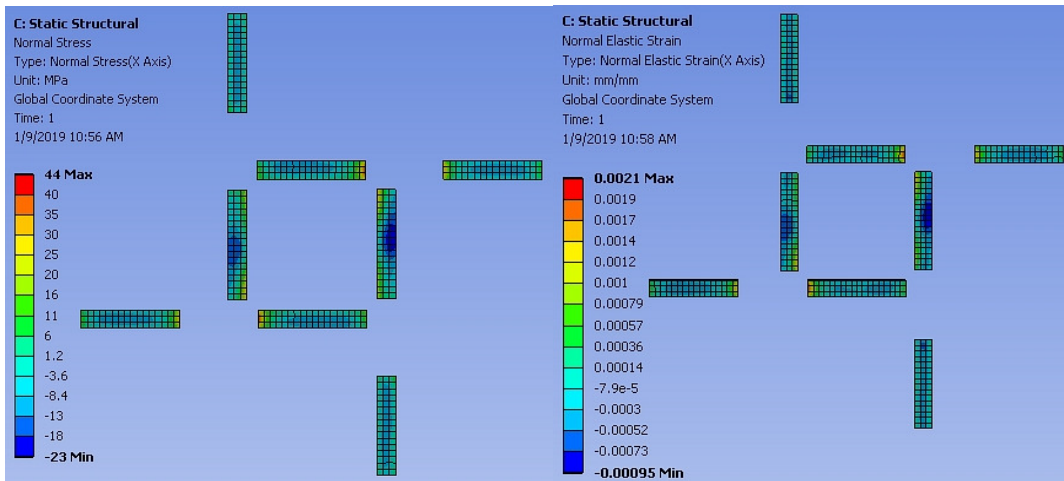


Figure 41: X-direction normal stress (left) and strain (right) on the coils.

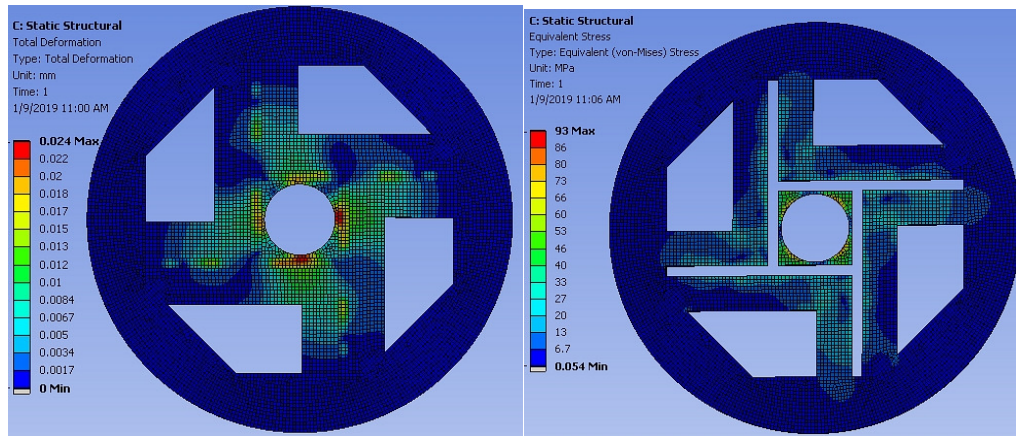


Figure 42: Deflections (left) and von Mises equivalent stress plots of simpler magnet support structure.

Symmetric Design

A similar analysis has been performed for the *symmetric* design. The boundary conditions for this case are simpler. The magnetic field is normal to the mid-plane, and the perpendicular displacement on the mid-plane is zero. Fig. 43 shows the displacement contour plot, which indicates that the maximum displacement occurs at the coils. The maximum displacement is only 9.3 μm , which is quite acceptable. Fig. 44 shows the von Mises stress for this design. The region with the largest stress is on the collar in the vicinity of the space between the coils. The strain associated to the von Mises stress is shown in Figure 45. The strain in the coil is shown in Figure 46. The peak values of displacement, stress and strain for the symmetric design are summarized in Table XV.

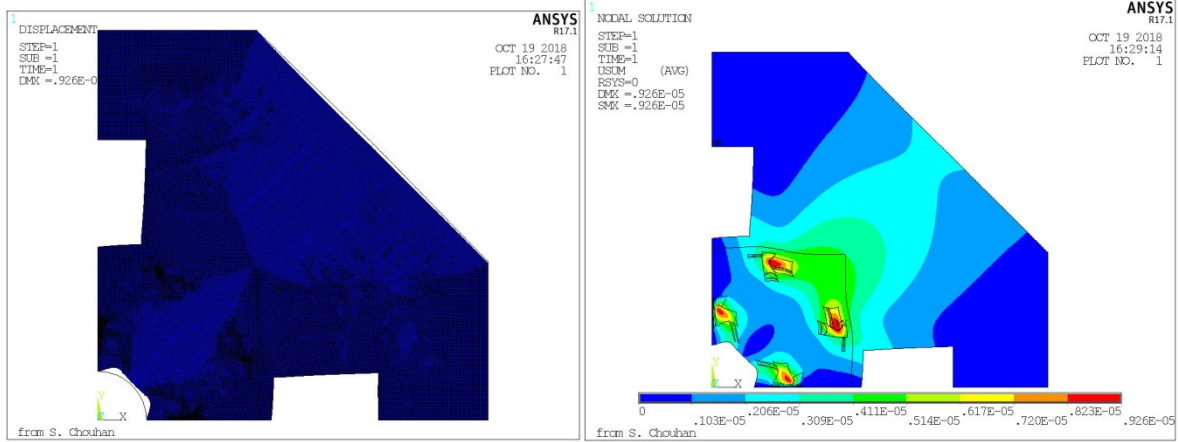


Fig. 43: Nodal displacement plot for the symmetric design. Left: Comparison of distorted magnet to the undistorted magnet. Right: Contour plot of nodal displacements.

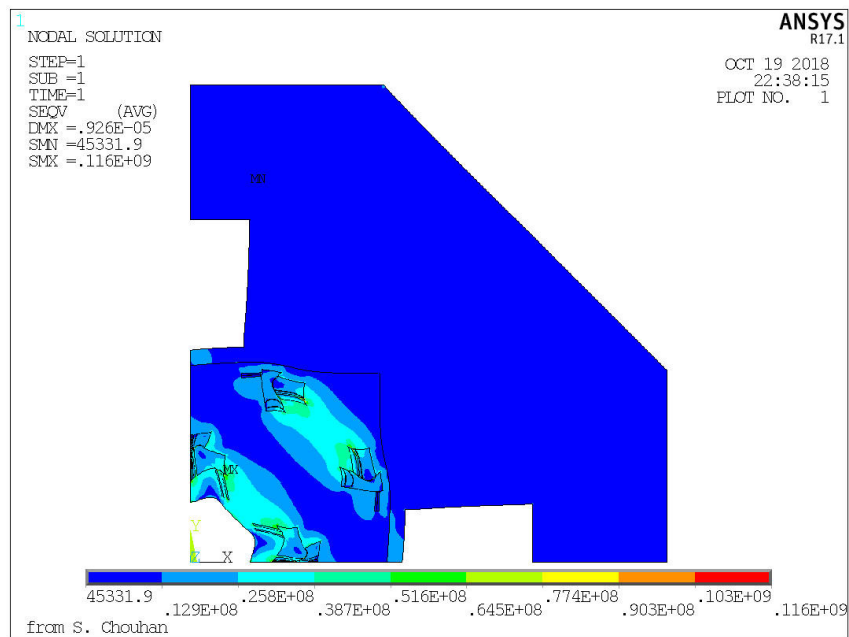


Fig. 44: von Mises stress for the symmetric design.

Table XV

KEY PEAK STRUCTURAL VALUES FOR THE DESIGN CONSIDERED

	Simpler	Symmet- ric	Material Limit
Design	D	A	
Maximum Displacement (μm)	10.5	9.3	
Peak Stress on Collar (MPa)	95	116	215
Peak Stress on Coil	46	56	210
Peak Coil Strain	0.1%	0.13%	0.23% to 0.28%

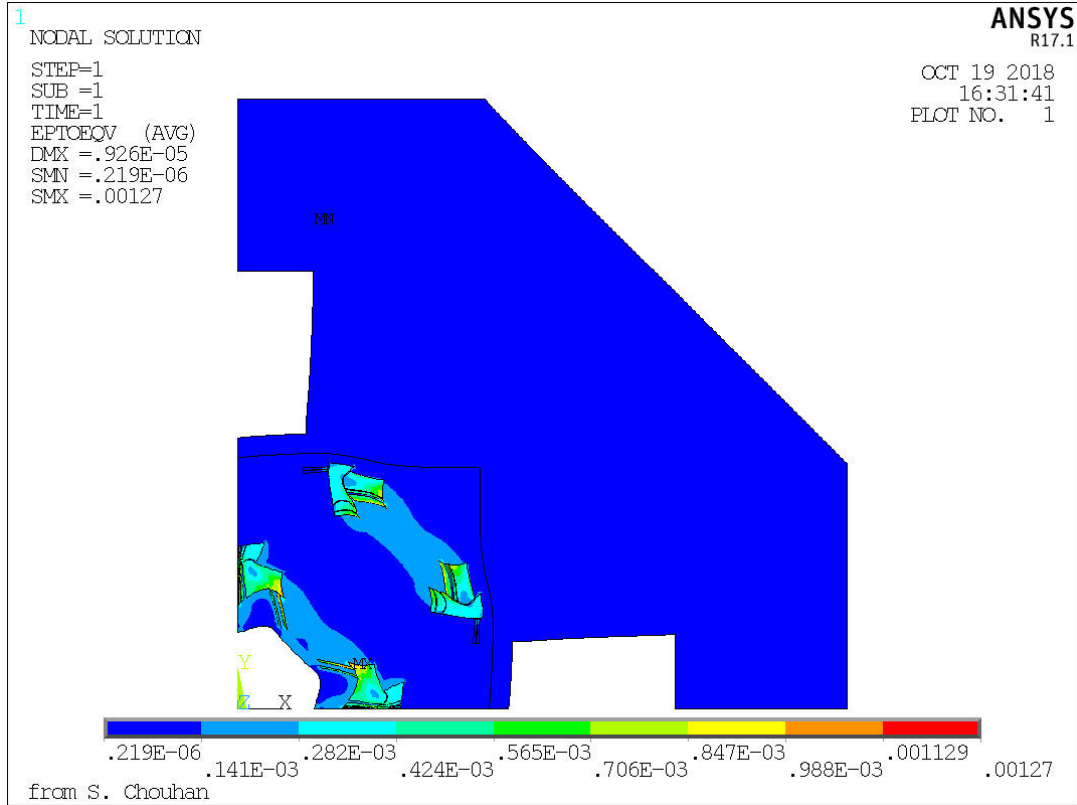


Fig. 45: Contour plot of the strain associated to the von Mises stress for the symmetric design.

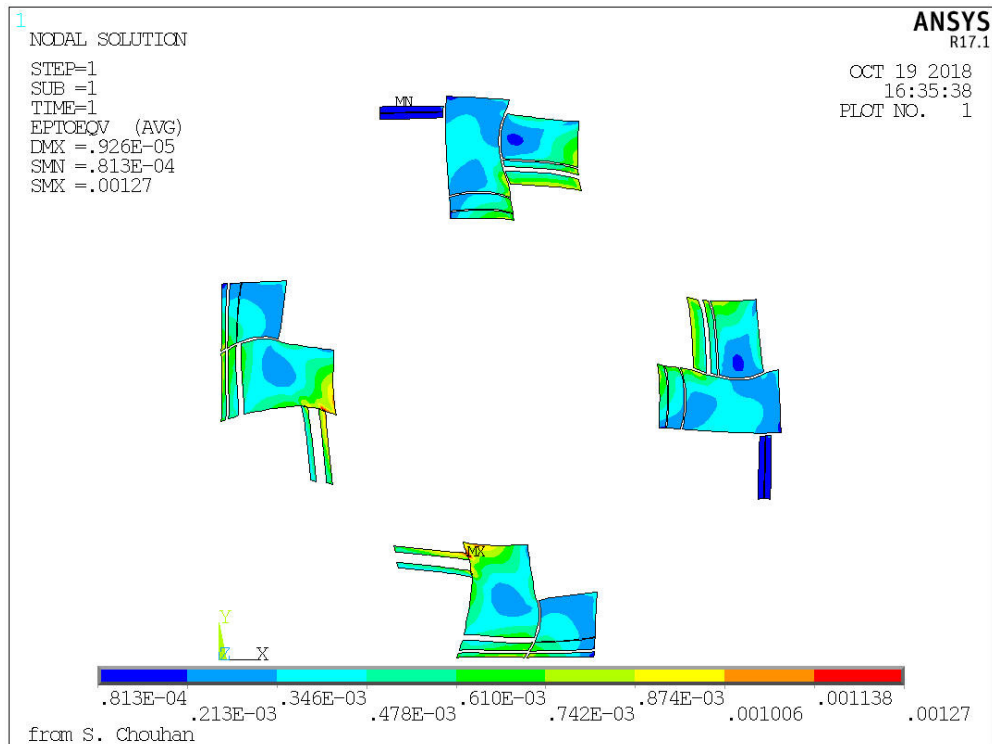


Fig. 46: von Mises strain in the coils for the symmetric design.

SECTION F: CONCLUDING REMARKS

We have examined designs using racetrack coils for the IR quadrupoles for both the eRHIC and JLeic EIC colliders. This modular concept where the magnet can be reconfigured by moving the racetrack coils can lower the costs of an R&D program to develop a new magnet where the parameters can change. In this case it has allowed us to use a single design with small modifications for both the eRHIC and JLeic IR quadrupoles. Two versions of the modular concept were studied: The *symmetric* version which has quadrupole symmetry and the *simpler* version which breaks that symmetry to make magnet fabrication and assembly easier.

There are advantages and disadvantages to each of these designs. The *simpler* design requires four simple identical racetrack coils. No interleaving between pancakes is required to assemble the magnet. Although the *simpler* design allows skew harmonics the skew quadrupole can be eliminated by rotating the magnet during installation. The higher order skew harmonics can be managed by minimizing the duo-decapole harmonic. This was shown to be feasible. In the design examined, the simpler design has higher saturation of the return yoke because of the close proximity of the coil to the iron. The *symmetric* design generally has smaller overall dimensions since the current return is split. The *symmetric* design allows the placement of the electron beam inside the iron flux return yoke which would supply partial shielding of the beam. In the simpler quadrupole design for the proton or ion magnets for the parameters examined, it was difficult to find a low field position for the electron beam in the *simpler* design. This may be overcome by using superconducting shielding around the electron beam [8].

We were able to achieve good field quality in all coil configurations examined. For the cable parameters chosen, the single layer coils carry more current and operate closer to the quench limit than the double layer design which operate at lower current and a healthy quench margin. We plan to optimize design parameters more in the Phase II where in addition to evaluating a wide range of parameters for studies, we will carry out the detailed magnetic, mechanical and engineering optimization of the designs with the parameters available at that time.

REFERENCES

- [1] L. Hand and W. Panofsky, "Magnetic Quadrupole with Rectangular Aperture", Review of Scientific Instruments, Vol. 30, Number 10 (1959).
- [2] A. Arno et al., "eRHIC Pre-Conceptual Design Report", Brookhaven National Laboratory, Upton NY, BNL Formal Report, BNL 205809-2018-FORE (2018).
- [3] R. Rajput-Ghoshal, R. Fair, P. K. Ghoshal, E. Sun, C. Hutton, M. Wiseman, "Preliminary Design of the Interaction Region Magnets for Future Electron-Ion Collider at Jefferson Lab.", Proc of ASC 2018 1LPo2J-02.
- [4] M. Wiseman, C. Hutton, F. Lin, V. Morozov, R. Rajput-Ghoshal, "Preliminary Design of the Interaction Region Beam Transport Systems for JLEIC", Proc. of ASC 2018.
- [5] R. Gupta et al., "Modular High Field Quadrupole Design for Electron-Ion Collider". Proc. of ASC 2018, 1LPo2J-12.
- [6] Stephan Russenschuck, Roxie magnet optimization program.
<https://espace.cern.ch/roxie/default.aspx>
- [7] P. Ferracin et al., "Development of a large aperture Nb₃Sn racetrack quadrupole magnet", IEEE Trans. Appl. Superconductivity, Vol 15, no. 2, pp 1132-1135, (2005).
- [8] R. Gupta et al., "Field Compensation in Electron-Ion Collider Magnets with a Passive Superconducting Shield", Proc. of ASC 2018, 2LPo2K-08.

APPENDIX: A

COIL WITH SPLIT TURNS DESIGN

Shailendra Chouhan

A new concept is proposed to achieve high field-gradient with low field region for the nearby electron beam. In the design, coil blocks are optimized angularly and radially in a manner that results in the desired high field gradient for ion beam and a large low magnitude fringe field area for the electron beam. This design has standard quadrupole boundary conditions (symmetry) and consequently there are no non-allowed normal (skew) harmonics present. Due to the large size of the electron beam pipe (diameter of 60 mm) and to contain the stray field magnitude in the electron beam region, the overall width of the coil is slightly wider compared to the known width of a cosine-two theta design magnet but is within present physical constraints. The advantage of the new concept is that there is no need of a bulky iron yoke or actively shielding coils. The main coil provides simultaneously the high-field gradient and the low field region. The superconducting coils were optimized within physical constraints while keeping field quality over the operating range. The optimized cross-section of the BNL Q1PF is shown above. To keep the simulation simple, rectangular coil blocks of realistic superconductor cross-section are considered. With the *split turns* coil design optimization is possible for a coil of any shape, including a cosine-two theta design as shown in Fig. A-2. Irrespective to the coil shape, this method provides a wide region of low field magnitude (in the range of 10^{-4} T) as shown in Fig. A-1 and Fig. A-2a.

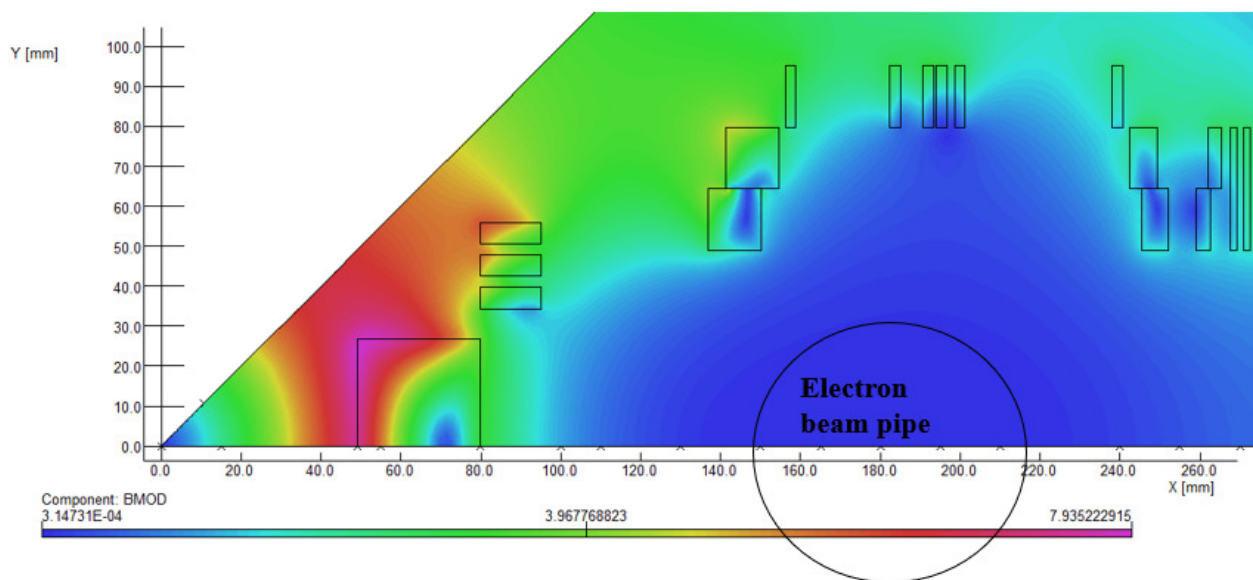


Fig. A-1. OPERA2d analysis of the split-turns design with field contour. The figure shows 1/8th of a model with symmetric boundary conditions. The location of the electron beam center is below the radially distributed coil block and is at 0.18 m from the magnetic center. Field magnitude in the range of 10^{-4} T.

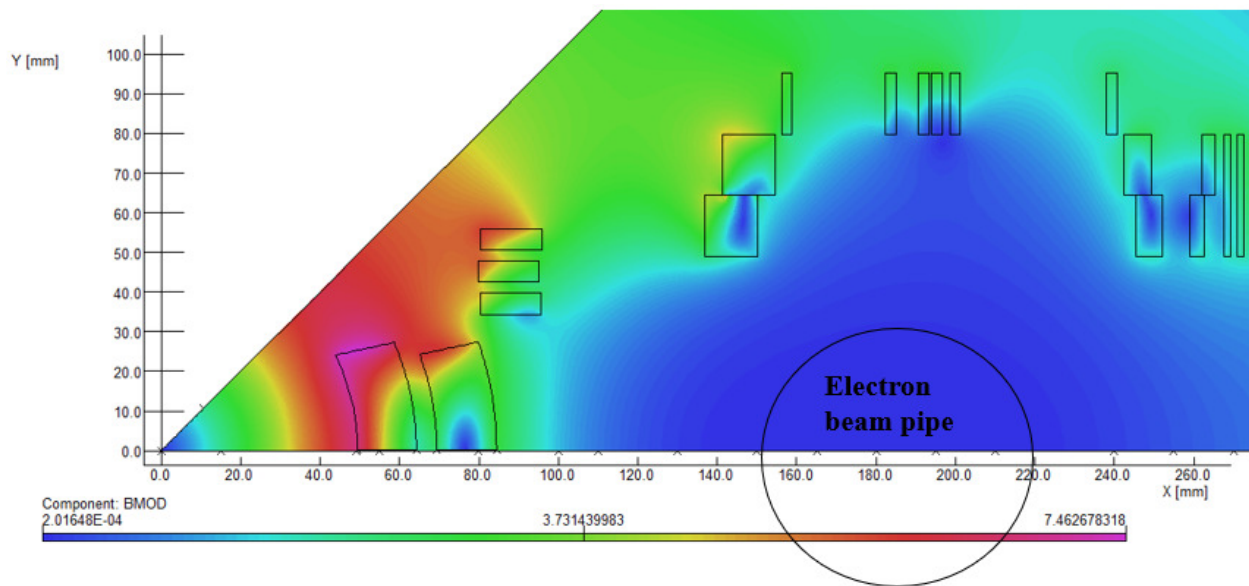


Fig. A-2a. OPERA2d analysis of the split-turns design with field contour. The figure shows 1/8th of a model with symmetric boundary conditions. The location of the electron beam center is below the radially distributed coil block and is at 0.18 m from the magnetic center. Field magnitude in the range of 10^{-4} T.

In both cases (Fig. A-1 and Fig. A-2) inner coil aperture is 96 mm and the achieved field gradient from the model is 140 T/m. It also shows a reduced field region for the electron beam enclosed by the circle (radius = 30 mm). The quadrupole field components (B_y and B_{MOD}) profile along the radial axis are shown in Fig. A-3. The linear field region in the center of the magnet provides the required high field gradient for the proton/ ion beam.

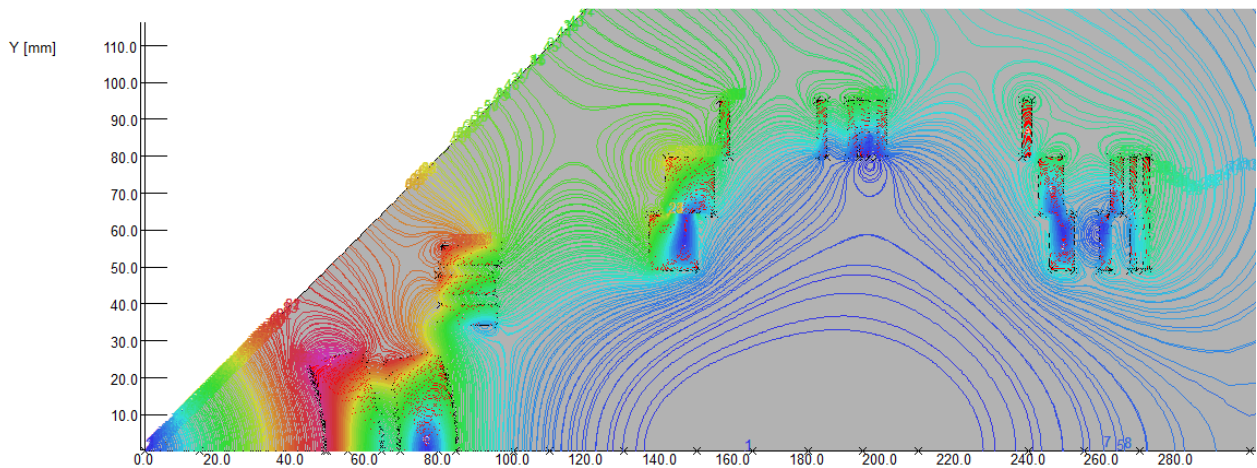


Fig A-2b: Magnetic flux, B_{mod} lines distribution with low field region for electron beam.

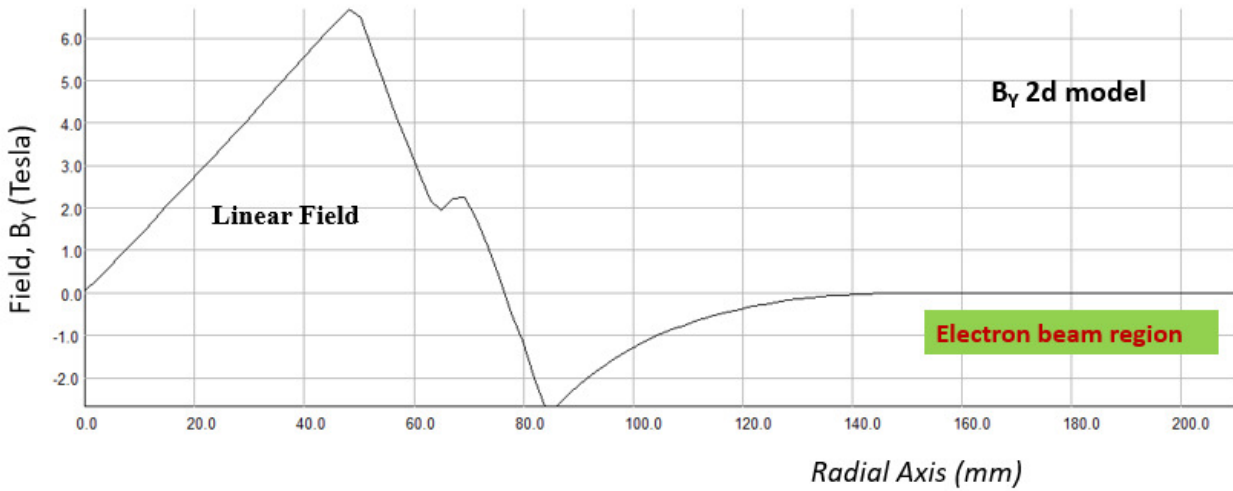


Figure A-3a. Calculated field, B_y (T) at mid-plane from 2d model along the radial axis. (Units are in millimeter and Tesla).

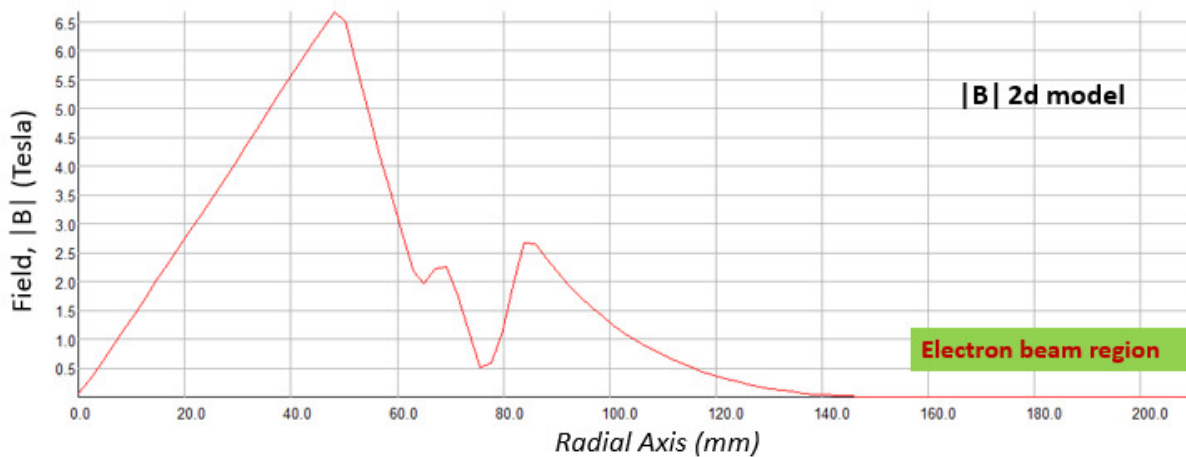


Figure A-3b. Calculated field, $|B|$ (T) at mid-plane from 2d model along the radial axis. (Units are in millimeter and Tesla).

Based on the 2d optimized design, the 3d modeling was performed. The 3D model provides an opportunity to examine the magnet in detail, especially the flux distribution along the ion/proton beam region, the stray field in and along the electron beam pipe, the peak field in the coil area, the integrated higher harmonic contents, and the forces on the coil, a magnetic model has been developed. Fig. A-4 shows the OPERA3D meshed model of the BNL_QIPF quadrupole with coils and the surrounding air region.

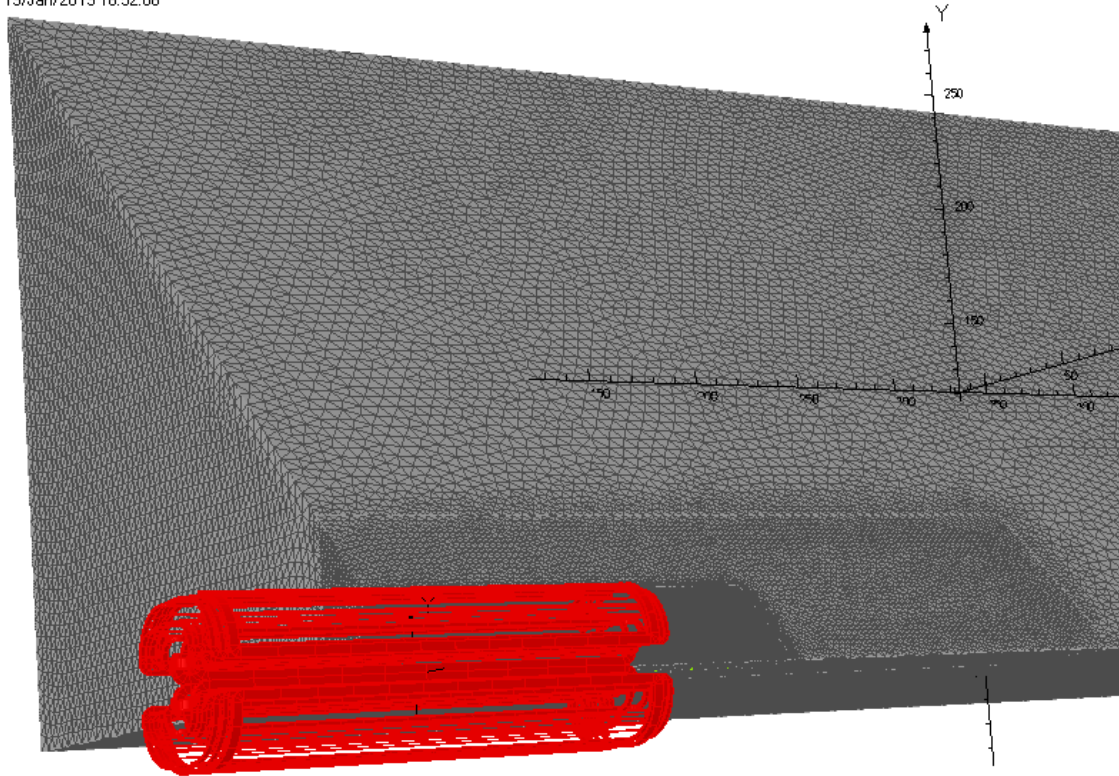


Figure A-4: 3d meshed model for the BNL Q1PF quadrupole magnet with superconducting coils with *Split turns* and background air.

The calculated field components, B_Y and $|B|$ profile at mid-plane along the radial axis from the 3d model are shown in Fig. A-5. Because the mid-plane axis is a quadrupole symmetry axis, consequently the resultant B_X component is zero. The calculated field profile along the longitudinal axis at a radius of 36 mm is shown in Fig. A-6. The calculated integral field strengths, $\int B_{2X} \cdot dL$ and $\int B_{2Y} \cdot dL$ at the reference radius of 36 mm are both 9.3 T·m and the resultant effective length, L_{eff} is 1.55 m. The calculated field profile along the longitudinal axis at a radius of 180 mm is shown in Fig. A-7. The calculated field magnitude in the center of the electron beam line is 5.0×10^{-3} Tesla and the integral field strength, $\int B_Y \cdot dL$ along the electron beam axis is 8.1×10^{-3} T·m.

20/Jan/2019 14:23:22

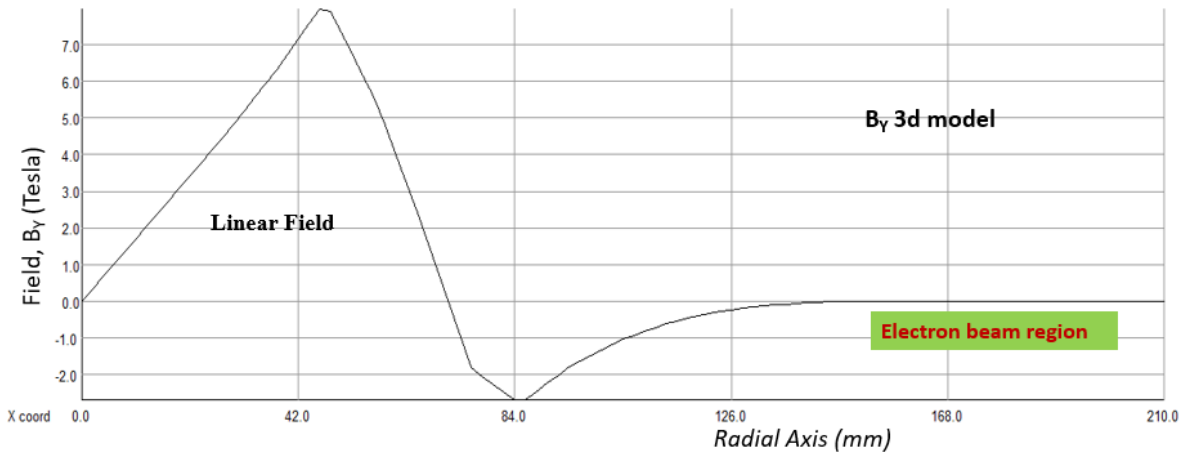


Figure A-5a. Calculated field, B_y (T) at mid-plane from 3d model along the radial axis. (Units are in millimeter and Tesla).

20/Jan/2019 14:27:18

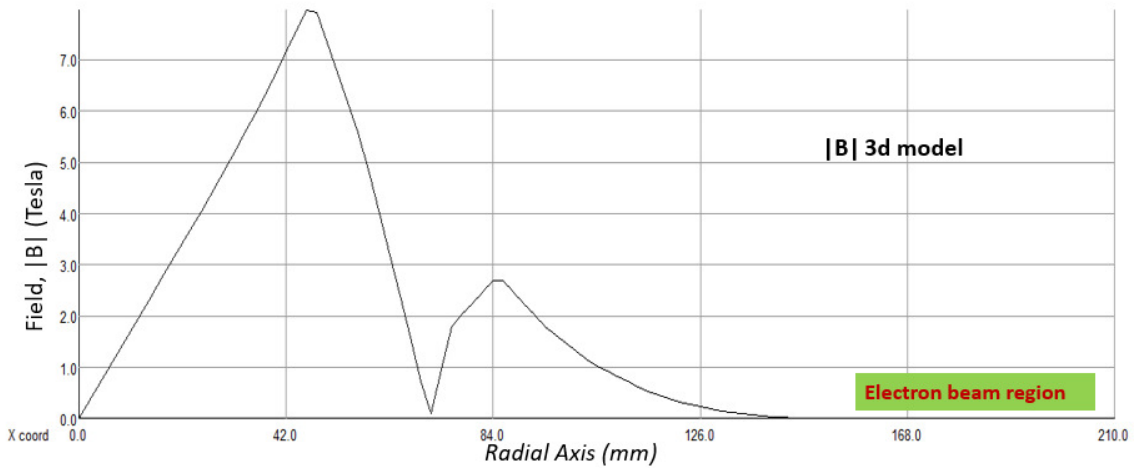


Figure A-5b. Calculated field, $|B|$ (T) at mid-plane from 3d model along the radial axis. (Units are in millimeter and Tesla).

20/Jan/2019 16:56:04

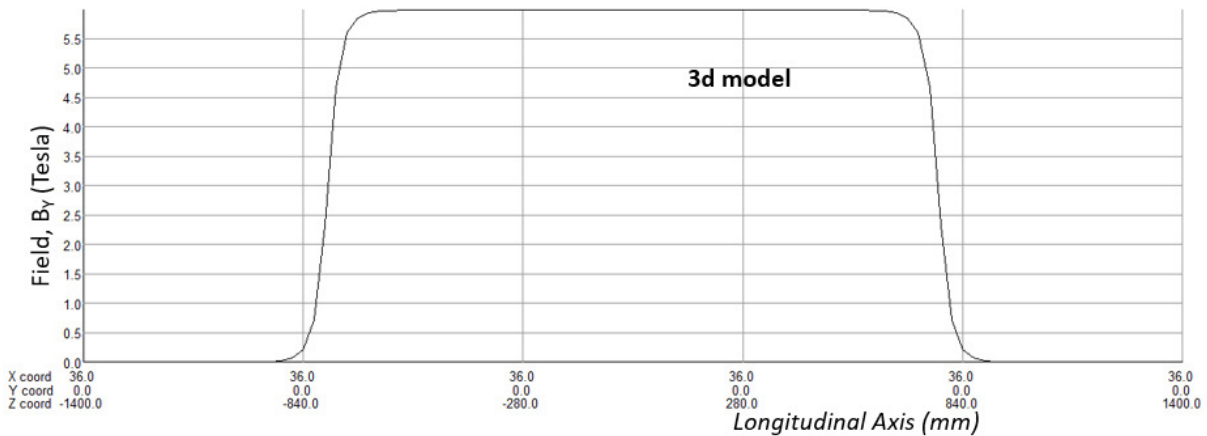


Figure A-6. Calculated field, B_y (T) at a radius of 36 mm along the longitudinal axis. (Units are in millimeter and Tesla).

20/Jan/2019 16:58:52

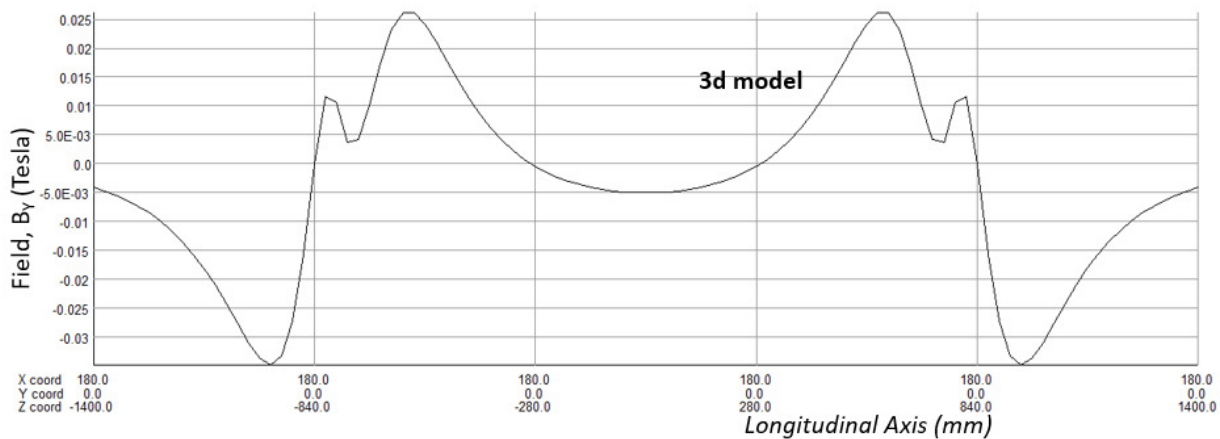


Figure A-7. Calculated field, B_y (T) at a radius of 180 mm along the electron beam axis. (Units are in millimeter and Tesla).

In order to further reduce the field magnitude in the electron beam region a 2.0 mm thick magnetic tube (1010 steel) is considered in the model. Fig. A-8 shows the exploded view of *split-turns* coil in the first quadrant with 2.0 mm thick magnetic tube around electron beam pipe. The field magnitude reduces significantly to $\sim 5.0 \times 10^{-4}$ T in the electron beam region as shown in Fig. A-9.

The 3d model is optimized to achieve 168 T/m (140 T/m + 20% margin). Around ten-percent additional current is required to achieve 168 T/m. The required operating current for a 168 T/m field gradient is 9.9 kA which is around 45% of the 8.7 T critical current field in the conductor. The design provides ample operation and safety margin. The field on the coil surface is shown in Fig. A-9. The peak field on the coil from the 3D program is ~ 8.7 T which occurs on the surface close to the pole where most of flux concentration takes place.

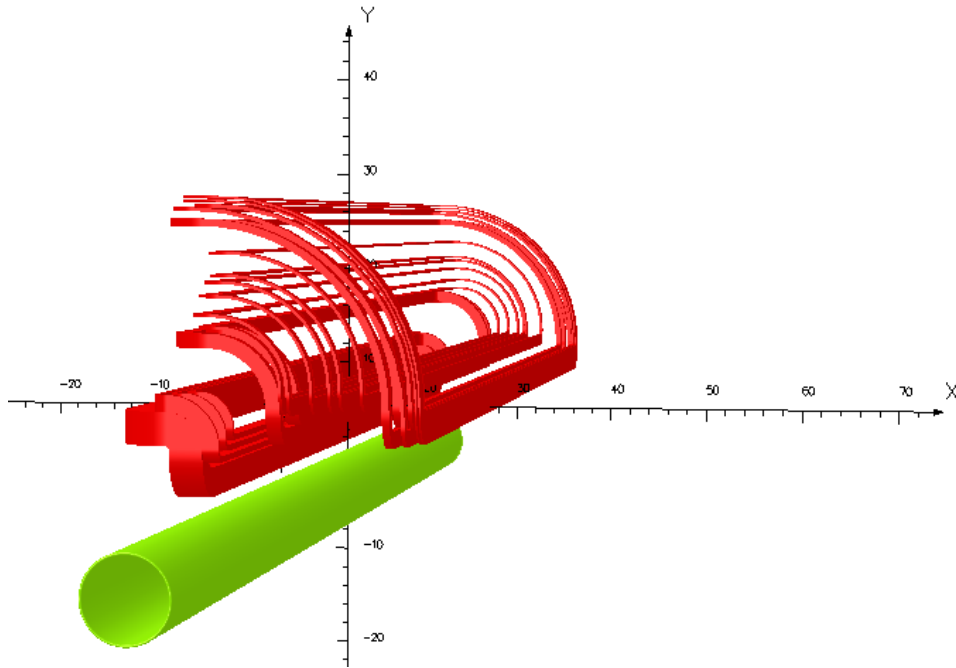


Figure A-8: 3d model of the superconducting coil with split-turns in the first quadrant along with magnetic tube around the electron beam.

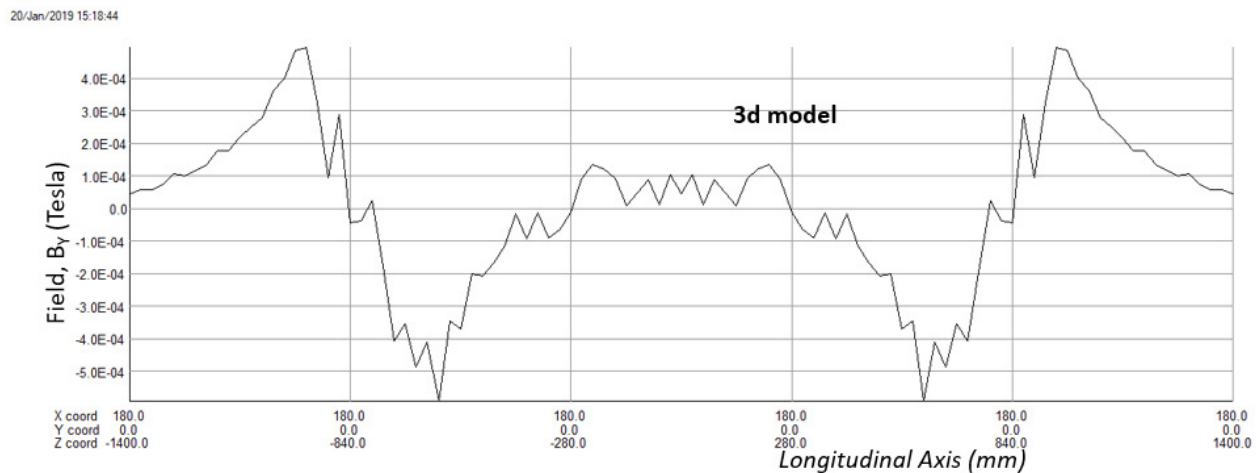


Figure A-9. Calculated field, B_y (T) at a radius of 180 mm along the electron beam axis. (Units are in millimeter and Tesla).

The advantage of this design over a *cosine-two theta* design with return yoke or actively shielded coils is that it has a naturally low field region (simp. A-2b), there is no need of bulky iron yoke, and no need to increase the current of the main coil to maintain the required field magnitude. Its advantage over a *Symmetric modular* design as discussed in section A and section B is that the new design has perfect quadrupole symmetry both in the center and at the end. In the *symmetric modular* design there is quadrupole symmetry in the center but at the end modules (pancakes) of the two orthogonal coils in each quadrant it must interleave and thus it breaks symmetry at the ends and generates higher order non-allowed harmonics such as octupole and its higher components. Whereas in the *simpler modular*

design prior rotation of the magnet (Fig. 31) is an essential precondition to minimize/ eliminate the skew quadrupole (and its components) and there is a non-zero torque, special provisions will be required in the cryostat to contain the rotational force. Additionally, in both designs even with iron return yoke, the fringe field magnitude is significantly high for electron beam (Fig. 17, Fig. 27) and the return yoke is highly saturated (Fig. 31).

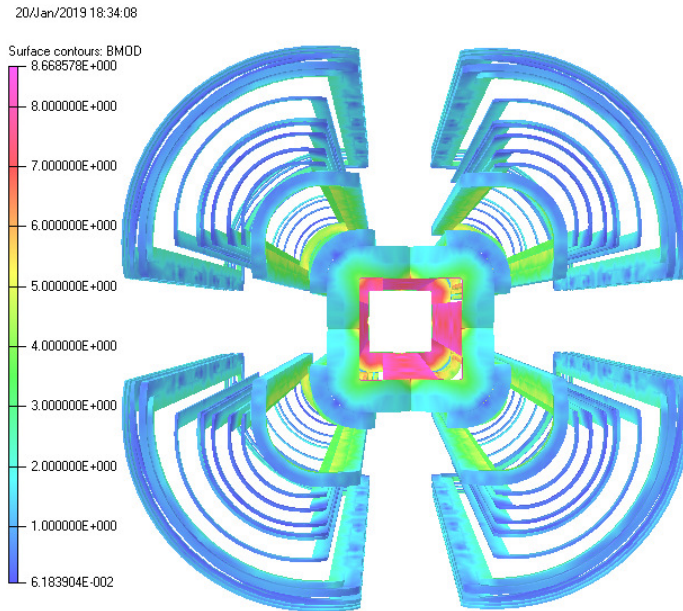


Fig. A-10: The 3D analysis provides the $|B|$ on the surface of the coils. The peak field occurs on the inner face where flux concentration is high. The large size opening at the mid-plane for the electron beam pipe.